NATIONAL ADVISORY COMMITTEE FOR AERONAUTICS

TECHNICAL NOTE 3453

LONGITUDINAL TURBULENT SPECTRUM SURVEY OF BOUNDARY

LAYERS IN ADVERSE PRESSURE GRADIENTS

By Virgil A. Sandborn and Raymond J. Slogar

Lewis Flight Propulsion Laboratory
Cleveland, Ohio

NACA

Washington

May 1955
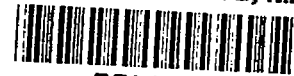
NATIONAL ADVISORY COMMITTEE FOR AERONAUTICS

TECHNICAL NOTE 3453

LONGITUDINAL TURBULENT SPECTRUM SURVEY OF BOUNDARY

LAYERS IN ADVERSE PRESSURE GRADIENTS

By Virgil A. Sandborn and Raymond J. Slogar

SUMMARY

Measurements of the longitudinal turbulent spectra for four stations in a turbulent boundary layer with increasing adverse pressure gradients are presented in tabular form.

Frequency diagrams show a decrease in the percentage of energy density contained in the high-frequency range as the flow continued down-stream against an adverse pressure gradient. However, the effect of pressure gradient was not pronounced; a similar redistribution of energy density occurred at a given station as the wall was approached.

Wave-number plots, on the other hand, show an increase in energy density in the large-wave-number range in the vicinity of the wall. The difference between the two plots is due to the mean-velocity factor in the relation between wave number and frequency.

The measured spectra are compared with the different variations predicted from the hypothesis of statistical equilibrium. Results tend to indicate that the predictions are consistent with the measurements at certain positions within the boundary layer.

The longitudinal-turbulence scales and microscales evaluated from the spectrum measurements are presented.

INTRODUCTION

Statistical theories of turbulence have been developed for homo-geneous and isotropic turbulence (ref. 1). For these comparatively simple motions it has been found that the flow field may be described in terms of defined statistical quantities, such as probability distribution functions, correlation functions, and energy spectral distributions. In general, it is possible to interrelate these statistical quantities mathematically or physically. While the turbulent motions encountered

in the field of aeronautics are more complicated than homogeneous turbulence, the studies of the simpler motions have indicated the terms that may be expected to be of major importance in a statistical theory of nonhomogeneous turbulence.

Since no complete statistical theory of turbulent shear flow exists at present, experimental research has been directed toward gaining an insight into the basic nature of the shear flow. Measurements of the intensity of turbulence alone have not yielded sufficient information about the flow fields. Thus, it is expected that investigations into the more complex quantities, such as correlations, spectra, probability densities, and terms of the higher moments of the equations of motion, for turbulent shear flows may lead to a fuller understanding of the non-homogeneous turbulence.

A significant theoretical concept developed for turbulent shear flow, Kolmogoroff's hypothesis of local isotropy (refs. 2 and 3), has been experimentally established by Townsend (refs. 4 and 5) and by Corrsin (ref. 6) for free turbulent shear flows.

In very recent measurements, attention has been directed toward the understanding of the fundamental transfer mechanisms of turbulent shear flows. The current approach is to evaluate all conceivable quantities in order to gain knowledge of the basic mechanism of turbulent shear flows. Corrsin and Uberoi (ref. 7) have explored the turbulent structure and the diffusion in a turbulent jet both for the verification of Kolmogoroff's local-isotropy hypothesis and to gain an understanding of the transfer of heat and momentum by turbulence. Townsend (ref. 8) and Klebanoff (ref. 9) have dealt with the turbulent-energy balance within turbulent boundary layers; their treatment has resulted in a fuller understanding of the mechanism and structure of this type of shear flow. Laufer (ref. 10) has investigated the rates of transfer, diffusion, and dissipation of energy in a fully developed turbulent pipe flow. The study of turbulence has been almost exclusively experimental, since no adequate theoretical model has been established.

This report is concerned with the measurement of spectra of the longitudinal component of turbulence at several stations in a boundary layer with varying degrees of adverse pressure gradient. The measurements are confined to stations upstream of the turbulent separation region and are in the region of the boundary layer where the turbulence signals are quite large. No measurements of spectra were made in the outer region of the boundary layer where the intermittency is of major importance.

The mathematical approach to representing a field of turbulent motion has been through Fourier analysis (ref. 1). A three-dimensional Fourier integral may represent a turbulent field. Experimentally it is

possible (by passing an electronic signal proportional to the velocity through a filter circuit, or wave analyzer) to make a Fourier analysis with respect to one space coordinate only. Or more precisely, it is possible to make a frequency analysis of the velocity components with respect to time at a fixed point. This frequency analysis can be assumed to be related to the wave-number analysis of the variation of velocity along a line in the direction of the stream. For homogeneous turbulence and certain specific conditions, it is possible to prove that the space average and the time average of fluctuating quantities are equal (ref. 11).

If the longitudinal turbulent-velocity fluctuation u is resolved into harmonic components, the temporal mean value of u^2 may be regarded as the sum of contributions from all frequencies. A spectral function $F(n)$ can be defined (ref. 12), so that $\overline{u^2}F(n)\,dn$ is the contribution of energy per unit mass from frequencies between n and $n + dn$. The total contribution from all frequencies is

$$\int_0^\infty F(n)\,dn = 1 \tag{1}$$

(A list of symbols is given in the appendix.)

The function $F(n)$ is the fraction of the total kinetic energy per unit mass of the turbulence arising from frequencies between n and $n + dn$, and may be thought of as the energy density at a given frequency.

It is possible to define a wave number as

$$k = \frac{2\pi n}{U}$$

(To associate this wave number with that used in theoretical considerations, the equivalence of space and time averages must be assumed.) The spectral function $f(k)$ can be defined so that $\overline{u^2}f(k)\,dk$ is the contribution of energy per unit mass from wave numbers between k and $k + dk$. The total contribution from all wave numbers is

$$\int_0^\infty f(k)\,dk = 1 \tag{2}$$

The following relation exists between $F(n)$ and $f(k)$

$$f(k) = \frac{U}{2\pi} F(n)$$

Both f(k) and F(n) can be interpreted as energy densities. The main
difference between the two representations of the turbulence spectrum
is that the k system is associated with a coordinate system in which
there is no mean motion with respect to the fluid, while the n system
is taken at a fixed point in a coordinate system where there is a mean
motion of the fluid. Physically, f(k) has dimensions of length, where-
as F(n) has dimensions of time. For a homogeneous flow (constant mean
velocity), it would make no difference whether f(k) or F(n) spectra
are discussed. In a shear flow, on the other hand, this relation is
affected by the mean velocity U.

In general, f(k) will be associated with physical eddies of turbu-
lence in the flow; thus, through the use of wave number, it is possible
to relate the existing theoretical work to physical measurements. How-
ever, any comparison with theoretical predictions must be made with
some reservations, since only the one-dimensional spectrum has been
evaluated and most theoretical work is based on a three-dimensional
spectrum.

The measurements reported herein constitute a phase of a long-range
research program directed toward the study of turbulent boundary-layer
separation. In general, the data are presented in tabular form, since
knowledge in the field has not progressed to a point where an adequate
analysis is possible.

APPARATUS AND PROCEDURE

Tunnel and test conditions. - The measurements reported herein were
made in the turbulent boundary layer along the test wall of the Lewis
6- by 60-inch boundary-layer channel. A schematic diagram of the tunnel
is shown in figure 1, and a complete description of the channel (except
a modified inlet) appears in reference 13. The channel inlet has been
reconstructed to take air from the large enclosed work area surrounding
the channel in order to eliminate fluctuations in mean velocity due to
atmospheric gusts. A honeycomb has also been added upstream of the
screens to reduce the possibility of secondary flows in the test section.
The addition of the honeycomb resulted in an increase of the free-stream
turbulence level from approximately 0.5 to 0.9 percent, which in turn
causes an appreciable thickening of the boundary layer. The effect of
the honeycomb may be seen by comparing the measurements presented in
reference 14 with those of the present report. With approximately the
same flow conditions at the inlet, the boundary layer at station 1 in-
creased from roughly 1.25 inches to nearly 2.00 inches after the honey-
comb was added. The measurements were taken at a constant Reynolds
number per foot of 2.9×10^5, which corresponded to a free-stream velocity
of approximately 49 feet per second, maintained at station 1 (fig. 1).

The suction through the porous wall (opposite the test wall) was suffi-
cient to keep the boundary layer along that wall at a constant thickness
(the same as reported in ref. 14 for the test with the 25-in. water-
pressure drop).

The four stations at which spectrum measurements were made are
spaced longitudinally approximately 18 inches apart, with the first
station located about 72 inches from the tunnel contraction, as shown
in figure 1. The boundary-layer thickness varied from about 2 inches
at the first measuring station to roughly 5 inches at the fourth station.
The adverse pressure gradient at each station is shown on the static-
pressure distribution curve (fig. 2).

Instrumentation. - The hot-wire-anemometer system used was the
constant-temperature system described in reference 15 with some modi-
fications within the amplifier made to reduce the noise level. A cut-
off filter at 16,000 cycles per second is employed in the hot-wire out-
put circuit to eliminate the noise signal for frequencies above 16,000
cycles per second.

A detailed description of the u-probe and of the system and tech-
nique of measurement with the constant-temperature hot-wire anemometer
are presented in reference 14. The hot wires were etched 0.0002-inch-
diameter tungsten with copper-plated ends. The unplated section was
0.040 inch long.

The frequency analyzer employed in the spectrum measurements was a
commercially available instrument with an adjustable band width. In
general, only the narrowest band width was used for the measurements.
An effective rectangular band width was defined from the experimentally
determined band shape, as shown in figure 3. In all but a few of the
measured spectra, the effective band width was 4.4 cycles per second.
For these few measurements, which were taken at a later date, a change
in a component of the analyzer circuit resulted in an increase of the
minimum effective band width to 11.7 cycles per second.

REDUCTION OF DATA

Mean-velocity profiles. - The mean-velocity profiles (fig. 4) were
evaluated from total-pressure profiles and the wall static pressure.
Details of the technique and equipment employed for the measurements
are reported in reference 14.

Longitudinal turbulent intensity. - The longitudinal-turbulent-
intensity distributions across the boundary layer at each station are
shown in figure 5. Details of the method employed to obtain these
measurements are also reported in reference 14.

Evaluation of spectral-density function. - The spectral-density
function F(n) was calculated from

$$F(n) = \frac{\overline{\Delta u^2}}{\Delta n \; \overline{u^2}} = \frac{\overline{\Delta e^2}}{\Delta n \; \overline{e^2}} \qquad (3)$$

where Δn is the effective band width of the analyzer, $\overline{\Delta e^2}$ is the mean
square voltage output of the analyzer between the frequencies $n + \frac{\Delta n}{2}$

and $n - \frac{\Delta n}{2}$, and $\overline{e^2}$ is the mean square of the total fluctuating wire
signal (read on an electronic average-square computer). A block
diagram of the instrumentation is shown in figure 6.

Through use of equations (1) and (3), a cross check on the instru-
mentation and data can be made in the following way. By plotting $\frac{\overline{\Delta e^2}}{\overline{e^2}}$

against n and integrating under the curve, it is possible to determine
an effective band width Δn, since, if Δn is independent of n,
equations (1) and (3) yield

$$\Delta n = \int_0^\infty \frac{\overline{\Delta e^2}}{\overline{e^2}} \, dn \qquad (4)$$

(where the upper limit ∞ was taken experimentally as 16,000 cps).
The values of Δn obtained from equation (4) varied randomly over an
appreciable range (the majority fell within a band of ± 20 percent from
the mean, but variations from the mean of ± 50 percent were also noted);
however, the numerical average value of Δn was 4.3 cycles per second,
as compared with the independently measured value of 4.4 cycles per
second. Thus, it is reasonable to assume that the experimental band
shape (fig. 3), which was determined mainly at 40 cycles per second
because of instrumentation restrictions, is a fair representation of
the analyzer's response at all frequencies.

In order to check for inconsistencies in the spectrum measurements,
equation (1) was evaluated for each spectrum (with a Δn of 4.4 cps).
Of the integrated values, 15 percent did not agree with equation (1)
within ± 0.2, while the other 85 percent scatter quite randomly about 1
with variations up to ± 0.2 being equally probable. A variation from
equation (1) of greater than ± 20 percent was assumed to represent more

than the expected random error of measurements, so that all data indicating an appreciably greater variation were discarded. It is believed that the larger variations resulted from foreign particles striking the wire during a spectrum measurement.

Evaluation of scales of turbulence. - Taylor (ref. 16) introduced a method of defining the average size of eddies as

$$L_x = \int_0^\infty R_x \, dx \tag{5}$$

where R_x is the correlation coefficient between the values of u at two points, separated by a distance x in the direction of the x-coordinate. The correlation coefficient R_x can be evaluated from the spectrum function $F(n)$ because R_x and $UF(n)/2\sqrt{2\pi}$ are Fourier transforms of one another (ref. 12). Therefore,

$$F(n) = \frac{4}{U} \int_0^\infty R_x \cos \frac{2\pi n x}{U} \, dx \tag{6}$$

and

$$F(0) = \frac{4}{U} \int_0^\infty R_x \, dx = \frac{4L_x}{U} \tag{7}$$

The first and third terms of equation (7) provide a convenient method of evaluating L_x. However, since no measurements below 20 cycles per second were recorded, the value of $F(0)$ can not be determined directly.

To determine a value of $F(0)$ from the measured data, the following method of extrapolation was used. From equation (6) it may be seen that the slope of the curve of $F(n)$ against n is zero at $n = 0$; therefore, the simplest logical approximation of the curve would be parabolic. A form of the parabolic equation given by Dryden (ref. 17) is

$$F(n) = \frac{F(0)}{1 + An^2} \tag{8}$$

For Dryden's particular flow, $A = 4\pi^2 L_x^2/U^2$ was used to determine $F(0)$. The value of $F(0)$ was determined by fitting equation (8) to points taken from faired curves passed through the measured points between $n = 20$ and $n = 100$ cycles per second.

Whereas L_x is related to the entire turbulent field, and in particular to the average eddy size, it is also possible to define

another length which can be regarded as a measure of size of the smallest eddies. This length λ_x, called the microscale, is defined (ref. 16) by:

$$\frac{1}{\lambda_x^2} = 2 \lim_{x \to 0} \left(\frac{1 - R_x}{x^2} \right) \tag{9}$$

In geometric terms, λ_x^2 is twice the radius of curvature of the correlation curve at $x = 0$. Thus, if the smallest eddies present in the turbulent flow are large, the correlation factor R_x would drop off slowly with x (large radius of curvature) and λ_x would be large, and conversely.

The microscale λ_x can be expressed in terms of the spectrum function $F(n)$ with the aid of the Fourier transform of equation (6):

$$R_x = \int_0^\infty F(n) \cos \frac{2\pi nx}{U} \, dn \tag{10}$$

If $\cos \frac{2\pi nx}{U}$ is replaced by the series $1 - \frac{2\pi^2 n^2 x^2}{U^2} + \frac{\pi^4 n^4 x^4}{12U^4}$ (as in ref. 12), the microscale becomes

$$\frac{1}{\lambda_x^2} = \frac{4\pi^2}{U^2} \int_0^\infty n^2 F(n) \, dn \tag{11}$$

The values of λ_x are determined from equation (11). The problem of defining the spectrum function at and near zero frequency is not of importance since the higher moment depends mainly on the contribution of the higher frequencies.

ERRORS

The noise level of the complete anemometer system is compared, in figure 7, with the longitudinal spectrum of turbulence measured at $y = 1$ inch for station 1. This particular spectrum is the most sensitive to noise level of those taken at station 1. (The noise level plotted in fig. 7 is on a scale relative to the total output signal of the hot-wire turbulence signal at a point 1.0 inch from the tunnel wall at station 1. It should, therefore, not be compared directly with any of the other frequency diagrams.) In general, the noise level is of importance only for the very-high-frequency range, and then only if the

over-all turbulence signal is very low. (In some cases where the energy density was very low $\left(F(n) \sim 10^{-10}\right)$ the noise level may have been en- countered at as low a frequency as 5000 cps. Also, for a few of the spectra, amplification of the turbulence signal was not sufficient to raise the very-high-frequency part above the noise level of the wave analyzer.)

The selectivity characteristic of the wave analyzer resulted in large fluctuations of the output meter; these were due to unequal weighting of the turbulence signal over the analyzer band width coupled with the very sharp peak in response at the resonance point. It was necessary to damp the meter by large capacitance in order to make readings consistent. Thus, the nonlinear averaging of the meter and capacitance are expected to introduce some error into the measurements.

Some error is present in the very-low-frequency measurements, be- cause they depend on the accuracy to which the analyzer was balanced. The balance was affected by the length of "warm-up" time of the instru- ment and was found to drift slightly during the measurements. This error explains the somewhat large variation of $F(n)$ noted at $n = 20$ cycles per second for a few of the spectrum measurements.

No attempt was made to correct the measurements for the effect of wire length (0.040 in.), since the turbulence scales were quite large compared with wire length. Approximate calculations suggest, however, that the error due to wire length will be no greater than 10 percent, and of that magnitude, only near the wall where the scales are smallest.

Although it would be impossible to determine all errors, the over- all random scatter in the measurements can be indicated by evaluation of equation (1). The random error in the individual measurements would be expected, on the average, to be no greater than the ±20 percent ob- served in the evaluation of the integral.

RESULTS AND DISCUSSION

Longitudinal spectra of turbulence. - The measured longitudinal spectra of turbulence for different y distances are presented in table I for each of the four stations investigated. Also included with each spectrum is the value of the integral $\int_{0}^{16,000} F(n) \, dn$, as obtained when checks on the measuring consistency were performed.

In figure 8, a comparison has been made between the spectra at station 1 and station 4 for the same y distances. Data from station 1 can be regarded as representing the distribution for a zero pressure

gradient, while station 4 was in the influence of a strong adverse
pressure gradient. The general variation with y distance is similar
for the two boundary layers. A somewhat greater fraction of the total-
energy density of the turbulence is contained in the low-frequency range
for the boundary layers in the strong adverse pressure gradient, as
might have been inferred from the fluctuations observed in the same
region from total-pressure-probe measurements (ref. 14).

A decrease in the energy density F(n) in the high-frequency range
was observed as the flow continued downstream against the adverse pres-
sure gradient; a similar decrease occurred at a given station as the
wall was approached. This latter decrease appears rather abruptly in
the vicinity of the wall, as is evident from an examination of the lines
of constant frequency of figure 9. The distance from the wall where the
decrease occurs is somewhat greater for the larger pressure gradients.

Spectra at station 1 are compared in figure 10 with measurements
of the spectra reported by Klebanoff (ref. 9) for a zero-pressure-
gradient boundary layer similar to that at station 1. The same general
trend of the spectra removed from the wall was noted, even though the
respective distances for the spectra do not correspond. These spectra
have also been compared by wave-number plots in figure 11. The opposite
trends observed at the high frequencies and high wave numbers (figs. 10
and 11) are due to the mean-velocity factor in the relation $k = 2\pi n/U$.

Second moment of longitudinal turbulence spectra. - A comparison
of the energy spectra across the boundary layers is made in figure 12
where the second moment $n^2F(n)$ is plotted against n. The slope of
the second moment curves at n = 0 is zero; however, the scale of
figure 12 is too small to indicate this trend. These plots not only
emphasize the energies corresponding to the higher frequencies, but
also are of importance in expressing the viscous dissipation. (For
isotropic turbulence, Lin (ref. 18) finds the rate of viscous dissipa-

tion of energy to be $2\pi\nu \dfrac{\overline{u^2}}{U}\left[- n^2F(n) + 4\displaystyle\int_{\bullet}^{\frac{2\pi n}{U}} nF(n)\ dn\right].$) Two general

types of distribution, sharp peak for the spectra near the wall and a
broader rounding off of the curves for the outer part of the boundary
layer, are apparently associated with the inner and the outer regions
of the boundary layer and can be seen in figure 12. However, this
trend is not very distinct at station 4.

Turbulent scales. - The scales L_x evaluated from equation (8)
and the faired data are shown in figure 13. Although any conclusion

based on the results must be made with some reserve, since the evalua-
tion of L_x must be quite arbitrary, it does appear that the scale
decreases near the wall.

Figure 14 shows a typical measured spectrum compared with the curve
determined from equation (8). The curve obtained by using Dryden's
value of A in equation (8) and fitting the data at n = 20 cycles per
second is included in figure 14. Use of Dryden's form of the parabolic
spectra to evaluate L_x, where the data at n = 20 cycles per second
were used, results in values of the same order of magnitude as those of
figure 13. However, since this curve was formulated for isotropic tur-
bulence, it probably will not fit the measured spectra exactly, as is
evident in figure 14.

The values of λ_x obtained from equation (11) are shown in figure
15. Estimates for the outer portion of the boundary layer (with the
exception of station 4) give values of λ_x/L_x between 0.1 and 0.4, in
comparison with a value of 0.2 at the center of channel estimated from
measurements presented by Laufer (ref. 20). The trends of λ_x are
similar to those observed for L_x.

Correlation coefficient R_x. - The Fourier transform relation be-
tween R_x and $F(n)$ (eq. (10)) was employed to evaluate R_x at a dis-
tance of 0.005 inch from wall at station 1 (fig. 16). The calculation
of R_x is extremely sensitive to the increments of n chosen in the
integration when x is large, as increasing x results in increasing
the frequency of the cosine function. The value of L_x obtained from
the correlation curve and equation (5) was smaller than that given by
the spectrum curve and equation (8) but of the same order of magnitude.

Comparison with theoretical predictions. - It is possible to in-
pret the effects of inertia, pressure, and viscous forces acting within
a turbulent field by introducing the Fourier coefficient representative
of the field into the Navier-Stokes equations of motion (ref. 1). In-
ertia forces transfer energy from one part of wave-number space to
another without changing the total amount of energy associated with any
directional component of the energy; pressure forces transfer energy
from one directional component of the Fourier coefficient to another
(in the direction of isotropy); and the loss of energy by viscous dissi-
pation is more rapid for the small-scale components than for the large-
scale components. With this insight into the general flow of energy,
a hypothesis of statistical equilibrium has been developed (ref. 1).

Since the turbulence is (assumed to be) generated as large-size,
small-wave-number eddies, the action of inertial forces is such that it

transfers the energy to the high wave numbers and thus directs it to the region of viscous dissipation, while the effect of pressure forces eliminates any directional perference. From this, Kolmogoroff postulates a region in the high-wave-number, small-eddy range that is of a universal character. For shear flow, the assumption is that as energy is handed down the range of eddies, it loses any directional character, resulting in isotropic small-scale motion.

For the subrange of values of k where viscosity is unimportant and the eddies are statistically independent of the large energy-containing eddies, the spectrum function obtained from Kolomogoroff's hypothesis is found to vary as $k^{-5/3}$. Heisenberg's extension of Kolmogoroff's theory of equilibrium for the small eddies (ref. 21), with the assumption of a definite form for the exchange of energy between different wave numbers, yields a variation of the spectrum function proportional to k^{-7} for very large values of k. A study by Tchen (ref. 22) considering not only viscous dissipation and inertia transfer, but also terms identified as production, convection, and diffusion, also predicts the -5/3 and -7 power laws; in addition, a -1 power law is found to exist when the mean velocity of the fluid is small.

The data of stations 1 and 4 have been compared with the spectrum variations predicted by the various solutions of the universal equilibrium theory in figure 17. The predicted slopes have been arbitrarily fitted to the data in the regions where they might be expected to be valid. The experimental data appear to agree with the power-law prediction over fairly extensive regions; however, in many cases the scatter of the measurements may have resulted in undue agreement. For the outer region of the boundary layer, the -7 power law either fits the spectrum curves somewhere below the level of measurements, or was not present at all. A region of -5/3 power law is reasonable for each profile, with the region of largest agreement being found in the outer portion of the boundary layer (range approximately 400 to 2000 cps at station 1 and 100 to 1000 cps at station 4).

The conclusions of Tchen (ref. 22) that a region of -1 power law exists and refers usually to larger eddies than does the -5/3 law are consistent with the measurements of this study. (The region of agreement of the -1 power law is from 60 to 400 cps for station 1 and from roughly 40 to 100 cps at station 4.) In general, the -5/3 power law fits a greater portion of the spectrum curve in the outer region of the boundary layer than the -1 power law, which becomes important for the region near the wall. This trend was predicted by Tchen, since the mean velocity is small and the production function is important near the wall; the -1 power law would be expected to be of greater importance there. For the spectra very near the wall ($y = 0.005$ in.), the trends are somewhat less defined, indicating the turbulence Reynolds number may be too low for all conditions of equilibrium to be valid.

The shape of the spectra in the large-eddy range where equilibrium theories are not valid still can not be predicted (ref. 1, pp. 91). In general, it is only possible to state that the spectral distribution at low frequencies will be a function of the initial conditions, and that the large eddies appear to react only weakly with the smaller turbulence.

CONCLUDING REMARKS

Comparison of the spectral distributions for boundary layers in zero pressure gradients and large adverse pressure gradients indicates that the same general trends exist in both cases. The percentage of energy density contained in the high-frequency range was decreased as the boundary layer continued downstream into a large-adverse-pressure-gradient region.

Comparison of spectra in wave-number plots indicates an increase in the energy density for the high-wave-number range as the wall was approached. At high frequencies the opposite trend was observed in the frequency plots very near the wall.

The ratios of the longitudinal scale and the microscale of the turbulence for the outer region of the boundary layer were of the same order of magnitude as values observed at the center of a fully developed channel flow.

Measured spectra showed some agreement with the predicted variations found from the universal equilibrium theory at all positions. The extent of agreement of any one power law was found to be largely a function of position in the boundary layer.

Lewis Flight Propulsion Laboratory
    National Advisory Committee for Aeronautics
        Cleveland, Ohio, March 16, 1955

APPENDIX - SYMBOLS

The following symbols are used in this report:

A   constant

a   reference point

$\overline{e^2}$ mean square of the total fluctuating hot-wire voltage due to turbulence

$\overline{\Delta e^2}$ mean square voltage of hot-wire between the frequencies $n + \dfrac{\Delta n}{2}$ and $n - \dfrac{\Delta n}{2}$

$f(k)$ percent of turbulent energy $\overline{u^2}$ associated with k

$F(n)$ percent of turbulent energy $\overline{u^2}$ associated with n

$F(0)$ value of $F(n)$ at $n = 0$

k   one-dimensional wave number, $2\pi n/U$

L_x longitudinal turbulence scale

n   frequency

Δn effective band width of wave analyzer

p   static pressure at wall (atmospheric pressure - tunnel-wall static pressure at distance x)

p_r reference static pressure (atmospheric pressure - tunnel-wall static pressure at zero distance)

R_x longitudinal space velocity correlation coefficient between points a and a + x, $\dfrac{\overline{u_a u_{a+x}}}{\overline{u_a^2}}$

U   local mean velocity

U_1 mean velocity in free stream where viscous effects are unimportant

u   instantaneous turbulent velocity fluctuations in x-direction

$\overline{\Delta u^2}$ mean square turbulence velocity between frequencies $n + \dfrac{\Delta n}{2}$ and $n - \dfrac{\Delta n}{2}$

3555

x   distance along surface of test wall

y   distance normal to test wall

δ^* boundary-layer displacement thickness

λ_x longitudinal microscale of u-fluctuations

REFERENCES

1. Batchelor, G. K.: The Theory of Homogeneous Turbulence. Cambridge Univ. Press, 1953.

2. Kolmogoroff, A.: The Local Structure of Turbulence in Incompressible Viscous Fluid for Very Large Reynolds' Numbers. Comp. Rend., Acad. Sci. URSS, vol. XXX, no. 4, 1941, pp. 301-305.

3. Batchelor, G. K.: Kolmogoroff's Theory of Local Isotropic Turbulence. Proc. Cambridge Phil. Soc., vol. 43, pt. 4, 1947, pp. 533-559.

4. Townsend, A. A.: Experimental Evidence for the Theory of Local Isotropy. Proc. Cambridge Phil. Soc., vol. 44, pt. 4, Oct. 1948, pp. 560-565.

5. Townsend, A. A.: Local Isotropy in the Turbulent Wake of a Cylinder. Australian Jour. Sci. Res., ser. A, vol. 1, no. 2, June 1948, pp. 161-174.

6. Corrsin, Stanley: An Experimental Verification of Local Isotropy. Jour. Aero. Sci., vol. 16, no. 12, Dec. 1949, pp. 757-758.

7. Corrsin, Stanley, and Uberoi, Mahinder S.: Spectra and Diffusion in a Round Turbulent Jet. NACA Rep. 1040, 1951. (Supersedes NACA TN 2124.)

8. Townsend, A. A.: The Structure of the Turbulent Boundary Layer. Proc. Cambridge Phil. Soc., vol. 47, pt. 2, 1950, pp. 375-395.

9. Klebanoff, P. S.: Characteristics of Turbulence in a Boundary Layer with Zero Pressure Gradient. NACA TN 3178, 1954.

10. Laufer, John: The Structure of Turbulence in Fully Developed Pipe Flow. NACA TN 2954, 1953.

11. Ribner, H. S., and Tucker, M.: Spectrum of Turbulence in a Contracting Stream. NACA Rep. 1113, 1953. (Supersedes NACA TN 2606.)

12. Taylor, G. I.: The Spectrum of Turbulence. Proc. Roy. Soc. (London), ser. A, vol. 164, Feb. 18, 1938, pp. 476-490.

13. Sandborn, Virgil A.: Preliminary Experimental Investigation of Low-Speed Turbulent Boundary Layers in Adverse Pressure Gradients. NACA TN 3031, 1953.

14. Sandborn, Virgil A., and Slogar, Raymond J.: Study of the Momentum Distribution of Turbulent Boundary Layers in Adverse Pressure Gradients. NACA TN 3264, 1955.

15. Laurence, James C., and Landes, L. Gene: Auxiliary Equipment and Techniques for Adapting the Constant-Temperature Hot-Wire Anemometer to Specific Problems in Air-Flow Measurements. NACA TN 2843, 1952.

16. Taylor, G. I.: Statistical Theory of Turbulence, pt. II. Proc. Roy. Soc. (London), ser. A, vol. 151, no. 833, 1935, pp. 444-454.

17. Dryden, Hugh L.: A Review of the Statistical Theory of Turbulence. Quart. Appl. Math., vol. 1, no. 1, Apr. 1943, pp. 7-42.

18. Lin, C. C.: Remarks on the Spectrum of Turbulence. Proc. Symposia of Appl. Math., Vol. 1. Am. Math. Soc., 1949, pp. 81-86.

19. von Kármán, Theodore: Progress in the Statistical Theory of Turbulence. Proc. Nat. Acad. Sci., vol. 31, no. 11, Nov. 15, 1948, pp. 530-539.

20. Laufer, John: Investigation of Turbulent Flow in a Two-Dimensional Channel. NACA Rep. 1053, 1951. (Supersedes NACA TN 2123.)

21. Heisenberg, W.: Zur statistischen Theorie der turbulenz. Zs. f. Phys., Bd. 124, Heft 7/12, 1948, pp. 628-657.

22. Tchen, C. M.: On the Spectrum of Energy in Turbulent Shear Flow. Jour. Res. Nat. Bur. Standards, vol. 50, no. 1, Jan. 1953, pp. 51-62.

3555

TABLE I. - LONGITUDINAL TURBULENCE SPECTRA

(a) Station 1

Frequency, n, cps	Distance normal to test wall, y, in.						
	0.005	0.010	0.025	[a]0.150	0.250	0.500	1.00
	Mean turbulence velocity, $\sqrt{\overline{u^2}}$, ft/sec						
	4.12	5.30	4.97	3.58	3.36	2.96	2.22
	Local mean velocity, U, ft/sec						
	13.0	19.1	25.0	32.5	35.1	40.4	45.5
	$\int F(n)\,dn$						
	0.912	0.917	0.865	1.19	0.900	1.15	0.857
	Percent of turbulent energy, F(n)						
20	3.42×10^{-3}	3.45×10^{-3}	4.26×10^{-3}	5.71×10^{-3}	4.14×10^{-3}	3.75×10^{-3}	4.38×10^{-3}
40	3.54	3.21	3.60	3.43	3.28	2.75	3.32
60	3.17	3.21	3.30	2.59	2.28	2.16	2.01
80	2.69	2.39	2.72	2.14	2.05	1.36	1.82
100	2.48	2.39	1.54	1.61	1.28	1.31	2.01
150	2.07	1.85	1.26	9.50×10^{-4}	1.05	1.07	1.25
200	1.78	1.38	1.08	7.69	7.13×10^{-4}	7.69×10^{-4}	1.03
250	1.20	1.17	8.24×10^{-4}	5.35	5.68	6.28	9.58×10^{-4}
300	9.18×10^{-4}	9.16×10^{-4}	6.14	5.35	4.82	4.92	6.55
350	7.32	8.03	6.14	4.64	--------	--------	--------
400	5.66	5.95	4.36	4.00	4.01	3.26	5.50
450	5.17	5.05	3.83	2.38	--------	--------	--------
500	4.68	4.62	3.83	2.38	3.12	2.86	4.56
600	3.30	3.82	2.88	1.92	2.32	1.96	3.48
700	2.30	2.44	2.14	1.52	--------	--------	--------
800	1.47	2.15	1.99	1.34	1.31	1.50	1.64
900	1.08	1.61	1.63	1.03	--------	--------	--------
1,000	7.49×10^{-5}	1.20	1.33	8.56×10^{-5}	1.00	9.81×10^{-5}	1.15
1,500	2.27	3.43×10^{-5}	4.97×10^{-5}	5.01	4.4×10^{-5}	4.49	7.29×10^{-5}
2,000	7.32×10^{-6}	--------	2.46	2.91	3.28	2.46	3.84
2,500	2.64	5.94×10^{-6}	1.54	--------	1.45	1.57	1.92
3,000	1.36	2.44	5.51×10^{-6}	1.26	9.90×10^{-6}	8.50×10^{-6}	1.25
3,500	6.75×10^{-7}	1.37	4.36	--------	--------	--------	--------
4,000	3.42	7.04×10^{-7}	2.30	6.07×10^{-6}	4.01	3.08	8.29×10^{-6}
4,500	2.07	3.91	1.44	--------	--------	--------	--------
5,000	1.53	3.00	1.21	4.00	--------	--------	--------
6,000	4.68×10^{-8}	1.53	3.61×10^{-7}	1.67	1.54	1.66	1.15
7,000	1.69	5.15×10^{-8}	2.46	5.92×10^{-7}	--------	--------	--------
8,000	1.17	3.10	1.16	4.79	3.84×10^{-7}	2.42×10^{-7}	4.10×10^{-7}
9,000	7.57×10^{-9}	1.67	6.80×10^{-8}	2.43	--------	--------	--------
10,000	1.17×10^{-8}	9.52×10^{-9}	4.40	1.61	1.45	1.23	2.85
16,000	7.57×10^{-9}	9.52	1.71	1.61	5.68×10^{-8}	5.47×10^{-8}	1.82

[a]Band width, 11.7 cps.

TABLE I. - Continued. LONGITUDINAL TURBULENCE SPECTRA

(b) Station 2

Frequency, n, cps	Distance normal to test wall, y, in.						
	0.005	0.010	0.025	0.150	0.250	0.500	1.00
	Mean turbulence velocity, $\sqrt{\overline{u^2}}$, ft/sec						
	3.77	4.32	4.50	3.15	2.98	2.72	2.33
	Local mean velocity, U, ft/sec						
	13.7	18.3	23.0	30.0	31.9	36.2	41.6
	$\int F(n)\ dn$						
	1.20	1.03	1.15	1.07	1.05	0.871	0.807
	Percent of turbulent energy, F(n)						
20	6.58×10^{-3}	6.72×10^{-3}	1.01×10^{-2}	4.22×10^{-2}	1.42×10^{-2}	5.67×10^{-2}	1.68×10^{-2}
40	5.69	4.70	5.48×10^{-3}	5.92×10^{-3}	6.52×10^{-3}	4.86×10^{-3}	4.82×10^{-3}
60	4.87	3.62	4.51	4.36	2.90	3.42	3.04
80	4.11	3.43	2.83	3.02	2.70	2.91	2.96
100	2.99	3.05	2.60	2.64	2.50	2.44	2.30
150	2.22	2.04	2.14	1.78	1.79	2.23	1.63
200	1.72	1.75	1.64	1.34	1.33	1.64	1.38
250	1.57	1.48	1.12	1.14	1.20	8.26×10^{-4}	9.44×10^{-4}
300	1.29	8.08×10^{-4}	9.06×10^{-4}	8.84×10^{-4}	1.07	6.34	7.94
350	1.10	7.62	8.36	7.96	---------	---------	---------
400	6.48×10^{-4}	6.72	5.91	6.97	4.16×10^{-4}	5.46	5.02
450	5.12	4.73	6.50	5.00	---------	---------	---------
500	4.70	4.38	4.84	4.37	2.92	3.24	3.69
600	3.56	3.70	4.34	3.36	2.61	2.48	2.16
700	2.27	2.80	3.18	2.20	---------	---------	---------
800	1.74	2.27	2.34	1.74	2.02	1.48	1.64
900	1.16	1.26	1.99	1.65	---------	---------	---------
1,000	9.97×10^{-5}	7.88×10^{-5}	1.74	1.13	1.16	9.77×10^{-5}	1.05
1,500	2.69	2.69	5.15×10^{-5}	5.93×10^{-5}	4.79×10^{-5}	4.54	8.03×10^{-5}
2,000	6.00×10^{-6}	1.13	2.84	2.64	2.70	2.91	3.18
2,500	2.57	3.70×10^{-6}	1.37	1.94	1.63	1.34	2.12
3,000	9.24×10^{-7}	1.37	6.49×10^{-6}	9.73×10^{-6}	8.77×10^{-6}	9.91×10^{-6}	1.03
4,000	1.16	3.43×10^{-7}	1.62	5.50	3.70	3.08	4.88×10^{-6}
5,000	3.56×10^{-8}	1.48	5.82×10^{-7}	2.05	---------	---------	---------
6,000	1.50	1.13	2.60	5.92×10^{-7}	4.27×10^{-7}	5.85×10^{-7}	8.03×10^{-7}
7,000	8.89×10^{-9}	2.80×10^{-8}	7.71×10^{-8}	2.83	---------	---------	---------
8,000	5.70	1.79	5.14	1.94	1.07	7.28×10^{-8}	2.62
9,000	5.70	1.03	2.26	8.61×10^{-8}	---------	---------	---------
10,000	5.70	8.48×10^{-9}	1.62	4.84	7.25×10^{-8}	5.06	1.24
16,000	4.35	7.00	1.08	2.15	2.37	1.821	6.57×10^{-8}

TABLE I. - Continued. LONGITUDINAL TURBULENCE SPECTRA

(c) Station 3

Frequency, n, cps	Distance normal to test wall, y, in.								
	0.005	0.010	0.025	0.150	0.250	0.500	1.00	1.90	[a]2.9
	Mean turbulence velocity, $\sqrt{\overline{u^2}}$, ft/sec								
	3.72	4.31	4.50	3.60	3.53	3.50	3.35	2.64	1.16
	Local mean velocity, U, ft/sec								
	8.51	17.8	19.4	23.4	24.8	28.2	34.6	40.5	44.1
	$\int F(n)\,dn$								
	1.17	1.15	1.14	0.917	0.982	0.950	0.796	1.17	0.862
	Percent of turbulent energy, $F(n)$								
20	7.41×10^{-3}	8.81×10^{-3}	9.10×10^{-3}	1.07×10^{-2}	8.22×10^{-3}	6.94×10^{-3}	1.04×10^{-2}	7.35×10^{-3}	7.92×10^{-3}
40	7.75	7.86	5.12	5.67×10^{-3}	5.46	4.64	3.95×10^{-3}	5.81	4.33
60	4.86	4.54	4.23	3.55	3.86	3.44	2.63	3.83	3.44
80	4.36	4.08	3.18	2.52	2.05	2.80	2.74	3.54	2.64
100	3.02	2.83	2.27	2.07	1.90	2.24	2.74	3.00	2.51
150	2.45	1.81	1.88	1.19	1.62	1.73	1.23	1.84	1.51
200	1.78	1.26	1.36	9.85×10^{-4}	1.36	1.43	8.62×10^{-4}	1.72	1.04
250	1.28	1.02	1.06	7.98	9.12×10^{-4}	1.04	8.00	1.11	7.66×10^{-4}
300	7.58×10^{-4}	7.06×10^{-4}	6.76×10^{-4}	6.14	5.53	4.98×10^{-4}	4.84	8.17×10^{-4}	5.33
350	8.09	5.31	7.93	4.83	--------	--------	--------	--------	--------
400	4.84	4.30	5.67	3.68	3.17	4.55	3.18	4.59	3.65
450	4.07	4.17	4.70	3.19	--------	--------	--------	--------	--------
500	3.17	3.48	4.24	2.98	2.39	3.02	2.31	3.81	2.10
600	1.65	2.16	2.50	2.46	1.54	1.66	1.59	2.94	1.57
700	1.34	1.29	2.24	1.42	--------	--------	--------	--------	--------
800	1.02	1.02	1.32	1.28	1.30	1.25	1.04	1.65	9.77×10^{-5}
900	4.87×10^{-5}	7.87×10^{-5}	1.22	8.85×10^{-5}	--------	--------	--------	--------	--------
1,000	4.37	5.28	9.51×10^{-5}	7.17	8.22×10^{-5}	6.325×10^{-5}	6.19×10^{-5}	1.00	6.25
1,500	8.69×10^{-6}	1.02	2.72	2.20	2.89	3.203	3.96	3.83×10^{-5}	1.72
2,000	2.42	3.15×10^{-6}	9.19×10^{-6}	1.20	1.36	1.431	2.22	1.84	1.46
2,500	6.80×10^{-7}	1.02	3.81	6.29×10^{-6}	6.68×10^{-6}	1.17	1.58	1.38	7.66×10^{-6}
3,000	5.12	3.86×10^{-7}	2.50	2.66	3.02	9.37×10^{-6}	3.18×10^{-6}	6.86×10^{-6}	3.40
4,000	5.68×10^{-8}	6.16×10^{-8}	4.78×10^{-7}	9.47×10^{-7}	1.16	1.13	1.72	2.04	1.41
5,000	1.90	2.55	1.28	2.20	--------	--------	--------	--------	--------
6,000	8.43×10^{-7}	1.13	4.67×10^{-8}	9.90×10^{-8}	1.62×10^{-7}	2.42×10^{-7}	3.30×10^{-7}	3.80×10^{-7}	2.15×10^{-7}
7,000	5.36	5.04×10^{-9}	3.00	3.55	--------	--------	--------	--------	--------
8,000	5.36	5.04	1.42	3.55	3.41×10^{-8}	8.34×10^{-8}	8.34×10^{-8}	3.30	1.07
9,000	5.36	5.04	1.18	1.58	--------	--------	--------	--------	--------
10,000	5.36	5.04	9.52×10^{-9}	1.58	1.80	2.89	5.15	4.00×10^{-8}	1.07
16,000	5.36	5.04	7.52	1.58	1.80	2.29	4.39	2.00	7.03×10^{-8}

[a] Band width, 11.7 cps

TABLE I. - Concluded. LONGITUDINAL TURBULENCE SPECTRA

(d) Station 4

Frequency, n, cps	Distance normal to test wall, y, in.									
	[a]0.005	0.010	0.025	0.150	0.250	0.500	1.00	2.00	3.0	3.5
	Mean turbulence velocity, $\sqrt{\overline{u^2}}$, ft/sec									
	2.68	3.17	3.50	2.96	2.95	3.01	5.21	2.98	2.20	1.80
	Local mean velocity, U, ft/sec									
	6.95	8.69	11.12	15.5	16.4	19.3	23.0	29.7	36.1	38.3
	$\int F(n)\,dn$									
	0.880	1.06	1.14	0.917	1.08	0.983	1.06	1.04	1.22	1.04
	Percent of turbulent energy, F(n)									
20	7.38×10^{-3}	7.43×10^{-3}	1.26×10^{-2}	1.07×10^{-2}	1.02×10^{-2}	8.74×10^{-3}	6.70×10^{-3}	1.34×10^{-2}	1.03×10^{-2}	7.05×10^{-3}
40	6.10	1.06×10^{-2}	8.68×10^{-3}	6.47×10^{-3}	6.01×10^{-3}	6.63	6.13	7.25×10^{-3}	5.04×10^{-3}	6.01
60	3.24	9.08×10^{-3}	4.32	4.36	4.36	4.02	5.34	5.11	4.35	5.05
80	2.82	4.98	3.52	3.30	3.14	2.96	2.91	4.19	2.57	4.17
100	1.98	4.60	3.38	2.67	2.67	2.79	2.72	2.27	2.32	3.31
150	1.46	2.10	1.80	9.97×10^{-4}	1.98	1.54	1.47	1.67	1.02	1.82
200	1.18	1.78	1.30	9.10	1.09	1.10	1.33	6.70×10^{-4}	8.95×10^{-4}	9.22×10^{-4}
250	7.87×10^{-4}	9.70×10^{-4}	9.44×10^{-4}	8.25	6.22×10^{-4}	8.20×10^{-4}	9.80×10^{-4}	4.46	6.96	7.72
300	6.63	6.59	6.46	5.81	5.81	4.60	4.80	4.04	4.76	5.41
350	4.79	4.84	5.45	4.64	---------	---------	---------	---------	---------	---------
400	3.80	4.07	4.95	2.77	2.96	2.86	2.68	2.56	3.71	3.27
450	3.51	3.16	4.05	2.40	---------	---------	---------	---------	---------	---------
500	2.94	1.80	2.26	2.32	2.68	2.18	1.66	1.86	2.16	2.61
600	1.56	9.79×10^{-5}	1.57	1.68	1.13	1.38	1.49	1.67	1.25	2.21
700	1.19	5.36	9.52×10^{-5}	7.42×10^{-5}	---------	---------	---------	---------	---------	---------
800	8.78×10^{-5}	3.44	7.55	7.92	7.18×10^{-5}	7.12×10^{-5}	6.80×10^{-5}	9.75×10^{-5}	7.43×10^{-5}	1.07
900	8.78	2.46	4.60	5.58	---------	---------	---------	---------	---------	---------
1,000	7.39	1.77	3.27	4.75	5.16	4.04	5.62	6.13	5.79	9.39×10^{-5}
1,500	1.58	4.84×10^{-6}	7.58×10^{-6}	1.87	1.99	1.43	2.05	2.61	2.57	3.77
2,000	4.78×10^{-6}	8.44×10^{-7}	1.61	5.95×10^{-6}	7.45×10^{-6}	5.82×10^{-6}	1.22	1.16	8.07×10^{-6}	1.13
2,500	---------	2.84	9.51×10^{-7}	3.38	2.32	2.76	4.21×10^{-6}	4.75×10^{-6}	4.98	5.71×10^{-6}
3,000	1.03	9.72×10^{-8}	3.50	1.83	1.07	1.69	2.45	1.67	3.91	2.82
4,000	2.20×10^{-7}	2.73	4.95×10^{-8}	4.75×10^{-7}	2.72×10^{-7}	4.83×10^{-7}	4.37×10^{-7}	6.13×10^{-7}	7.43×10^{-7}	9.39×10^{-7}
5,000	6.64×10^{-8}	1.21	1.90	1.08	---------	---------	---------	---------	---------	---------
6,000	1.66	1.02	7.17×10^{-9}	4.05×10^{-8}	2.30×10^{-8}	5.54×10^{-8}	9.72×10^{-8}	9.39×10^{-8}	9.26×10^{-8}	1.26
7,000	8.78×10^{-9}	5.44×10^{-9}	7.17	2.50	---------	---------	---------	---------	---------	---------
8,000	5.46	5.44	7.17	1.68	1.32	1.46	3.03	2.90	3.15	5.11×10^{-8}
9,000	1.83	5.44	7.17	1.68	---------	---------	---------	---------	---------	---------
10,000	9.76×10^{-10}	5.44	7.17	1.32	1.32	1.46	1.94	1.04	2.32	3.76
16,000	3.22	5.44	7.17	1.32	1.32	1.46	1.94	4.65×10^{-9}	1.03	1.67

[a] Band width, 11.7 cps.

Suction-control
manifold

Porous-wall
suction compartments

Honeycomb

Screens

12

Porous wall

6

Air-flow
direction

Test wall

Station   4   3   2   1

Removable channel sections

Air
inlet

To
exhauster

18

72

60

Station
4   3   2   1

142

24

6

CD-4235
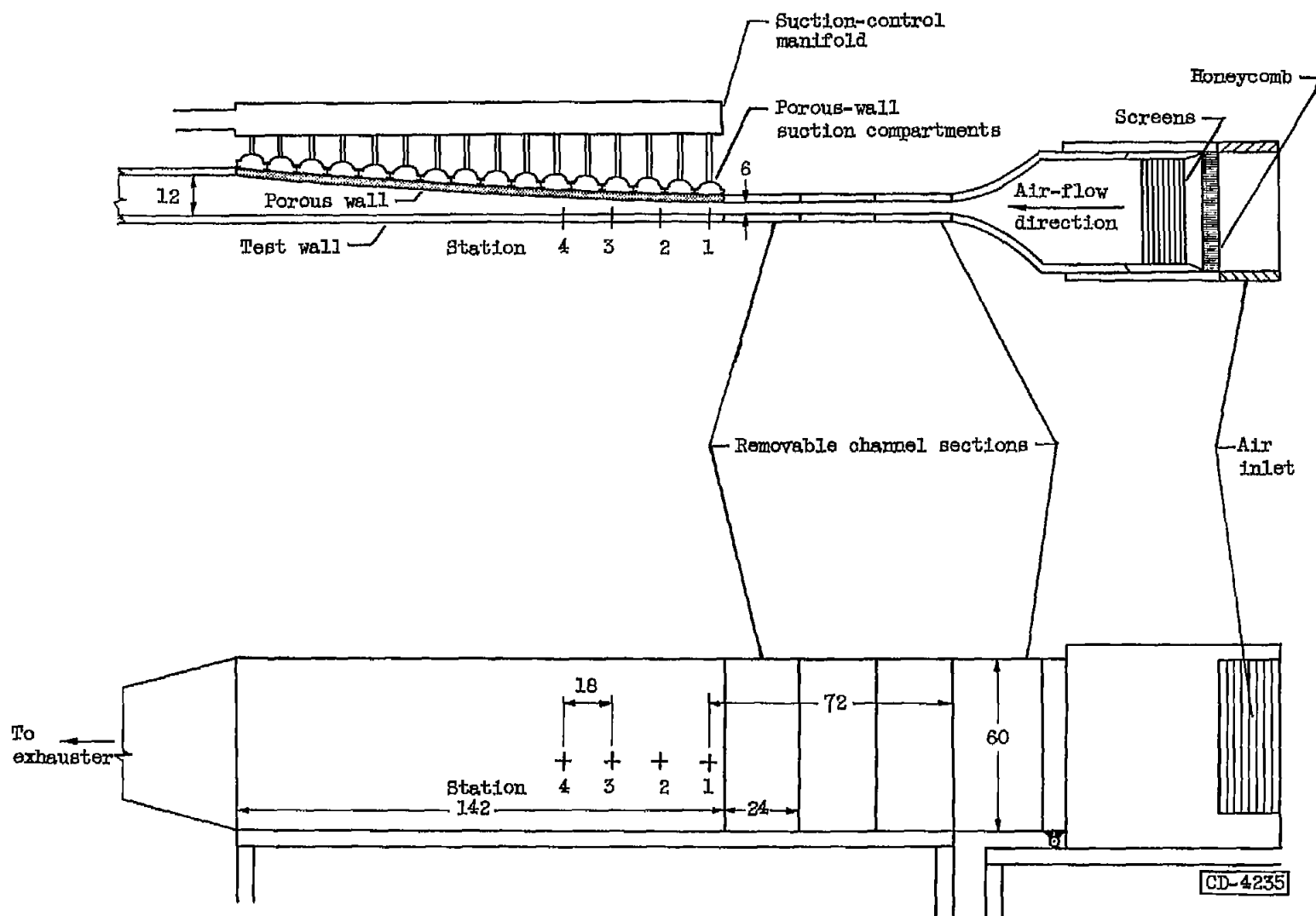
Figure 1.- Schematic diagram of 6- by 60-inch subsonic boundary-layer channel.
(All dimensions are in inches.)
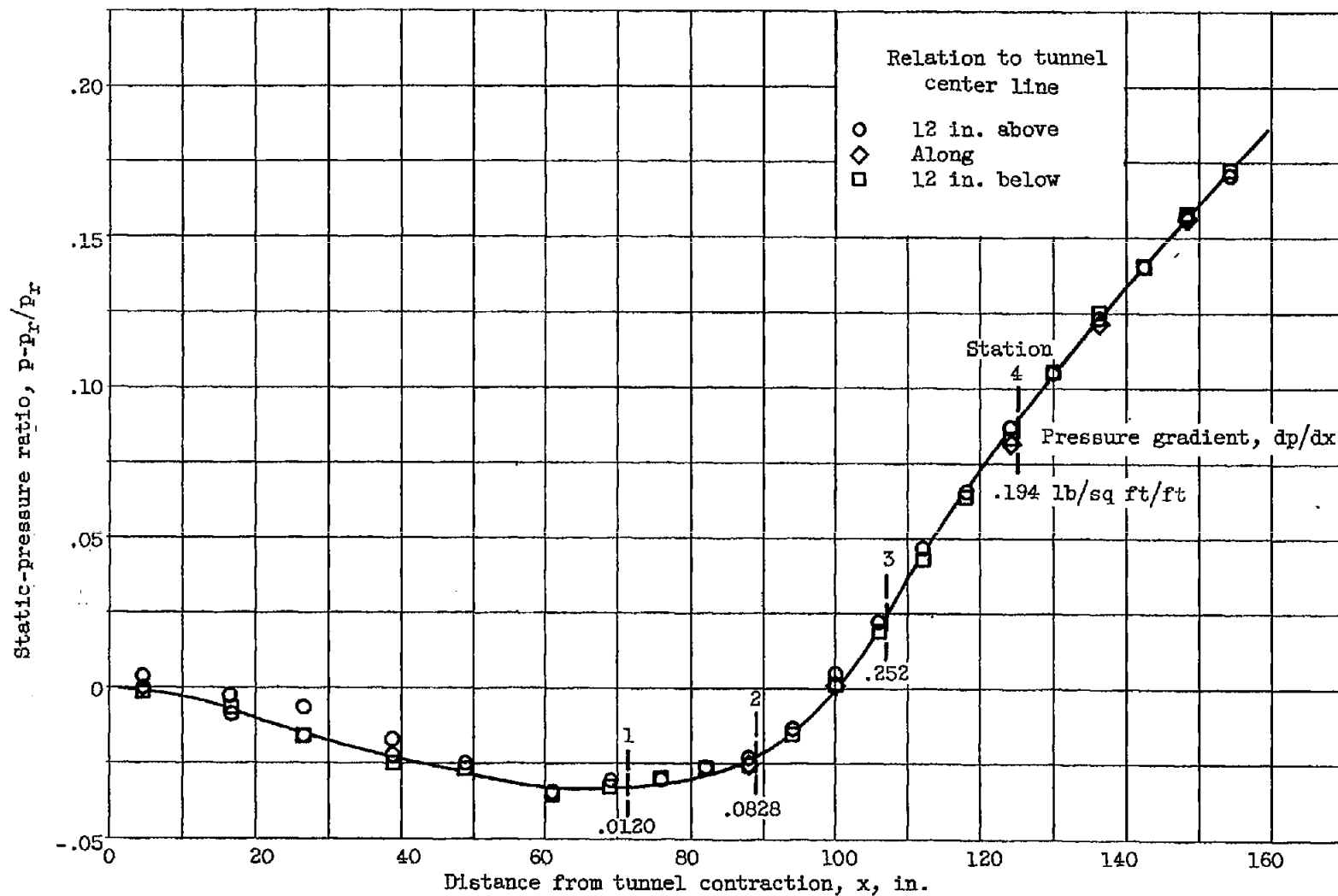
Figure 2. - Static-pressure distribution along tunnel wall. (p, static pressure at wall; p_r reference static pressure.)

Effective half band width at 40 cps

Resonance at

O   40 cps
□   400 cps

Ratio of outputs, $\text{output}^2/(\text{output}_{max})^2$

Cycles off resonance
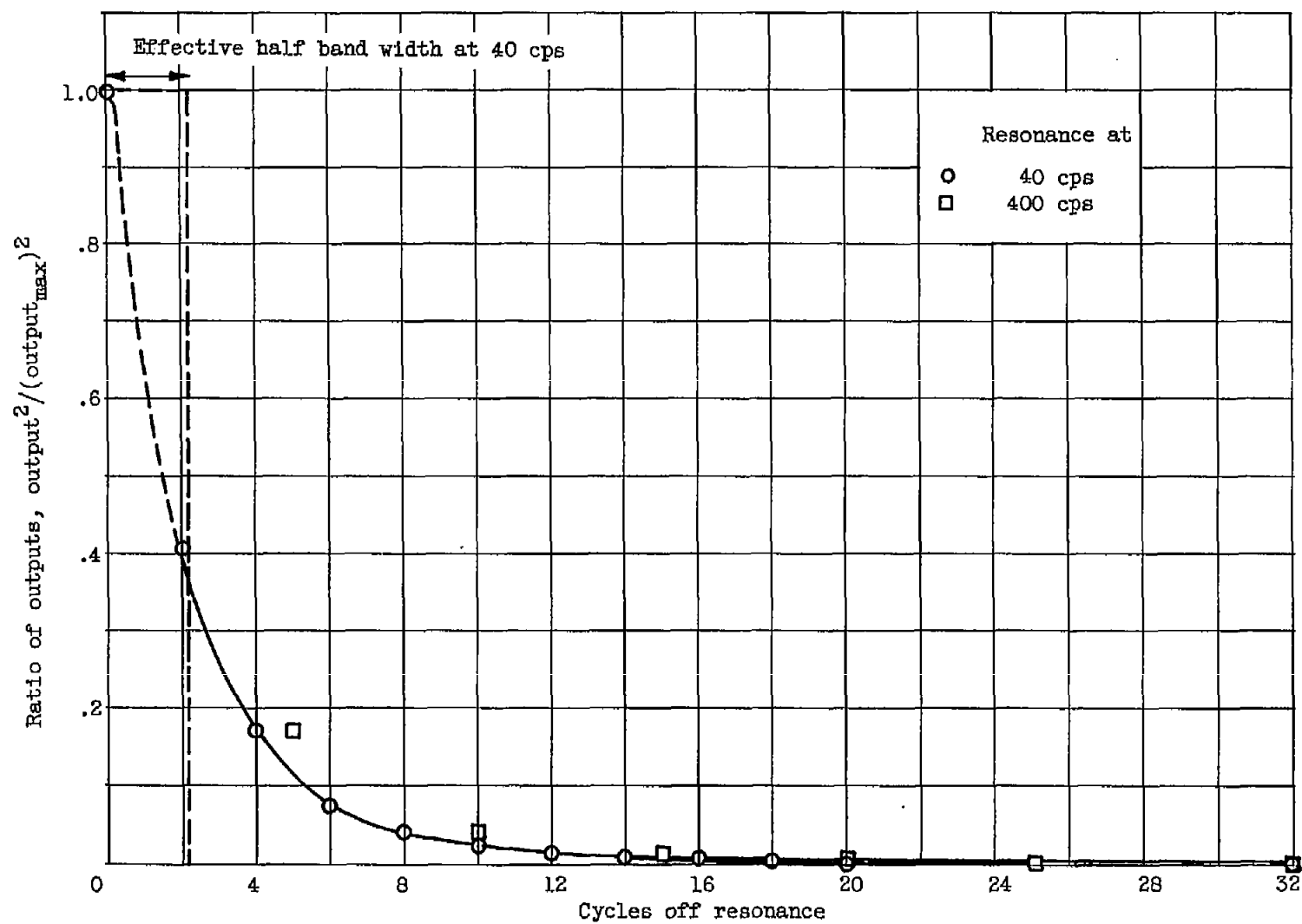
Figure 3. - Selectivity characteristics of harmonic wave analyzer. Area under rectangle equals
area under curve. (Frequencies plotted above resonance point.)
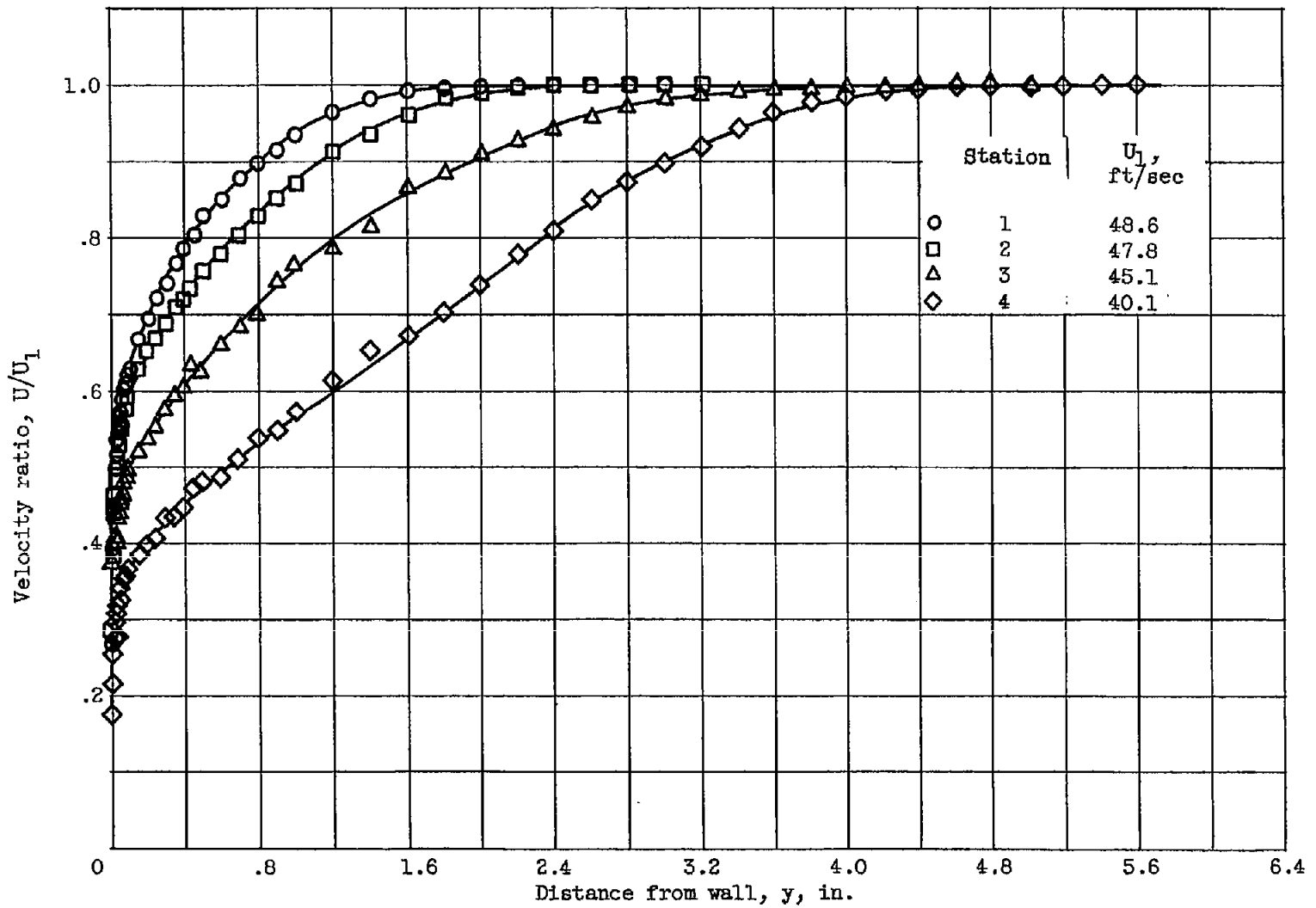
Figure 4. - Mean-velocity distribution through boundary layer.

3555

'CQ-4
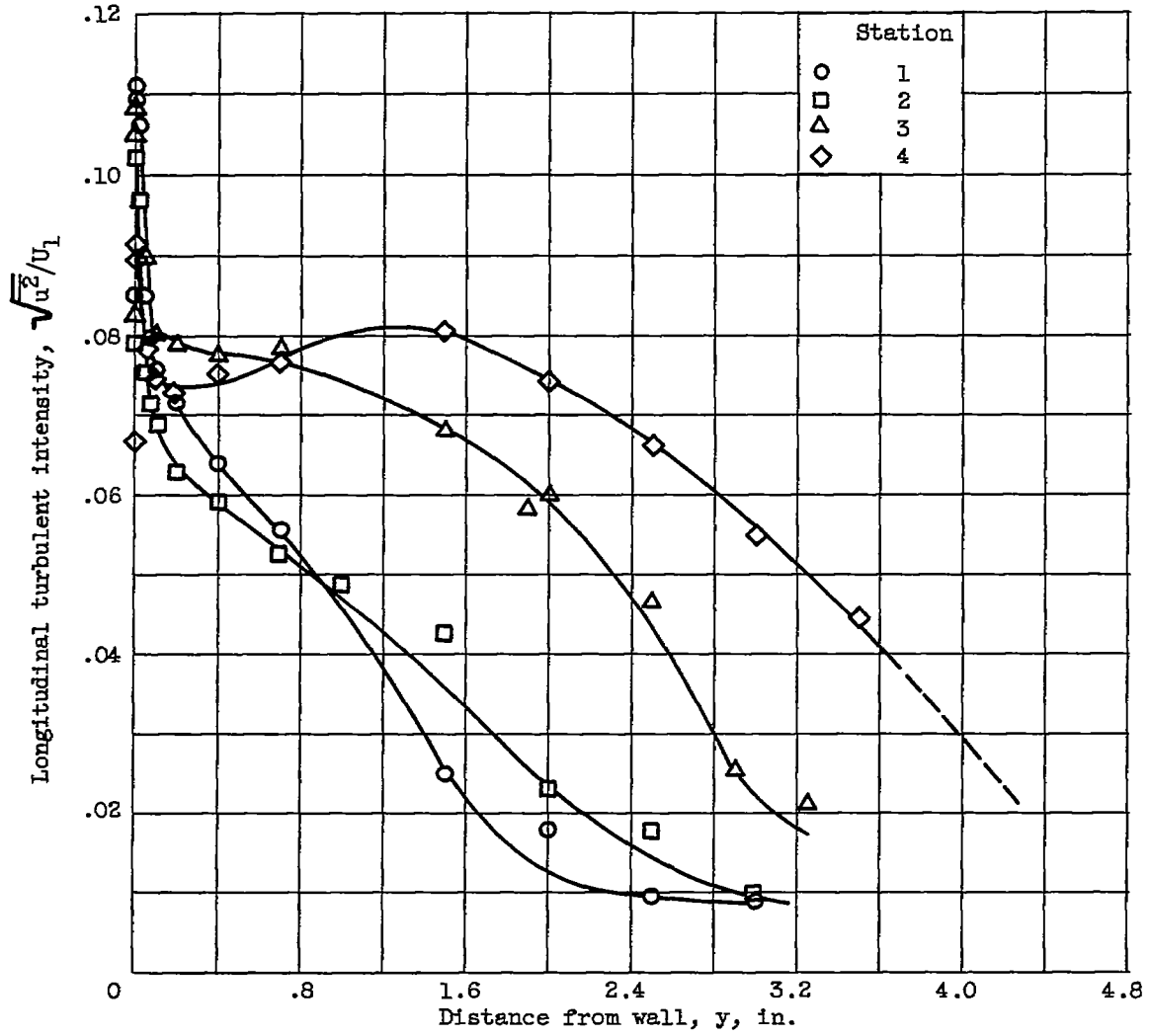
Figure 5. - Variation of longitudinal turbulent intensity across boundary
layer.
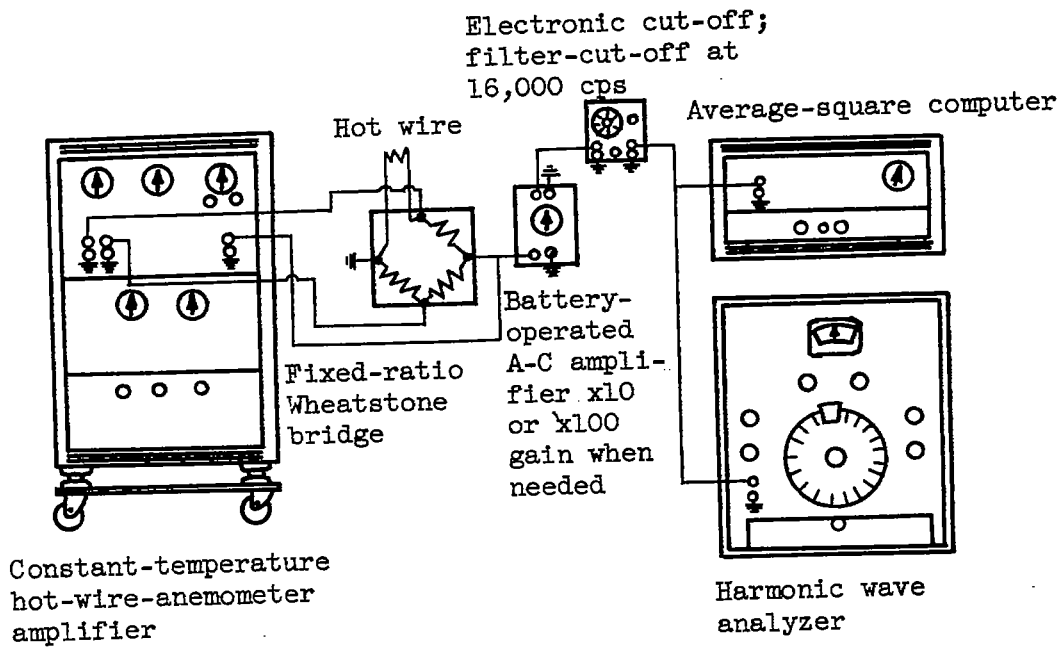
Figure 6. - Block diagram of instrumentation hookup.

3555

CQ-4 back
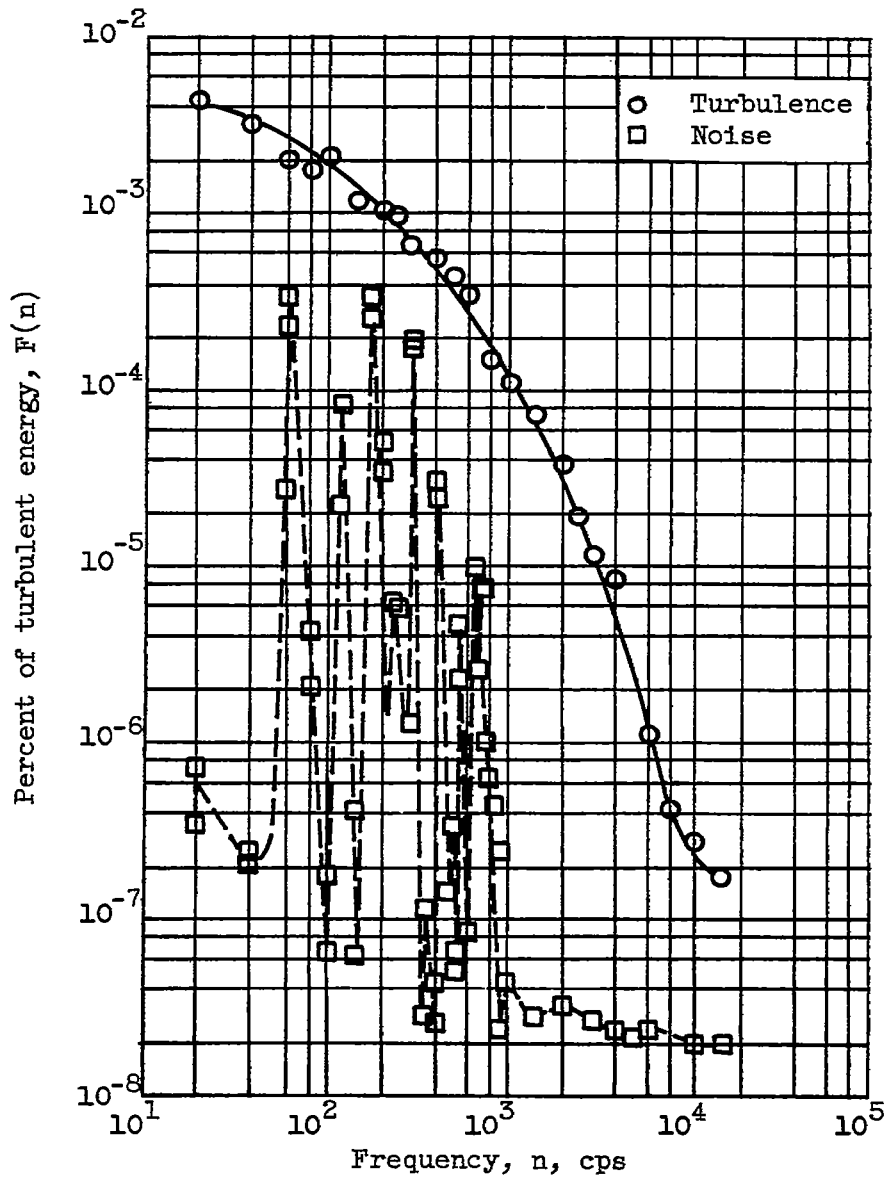
Figure 7. - Relative noise level of complete
anemometer system compared with measured
longitudinal turbulence spectrum 1.0 inch
from tunnel wall at station 1.
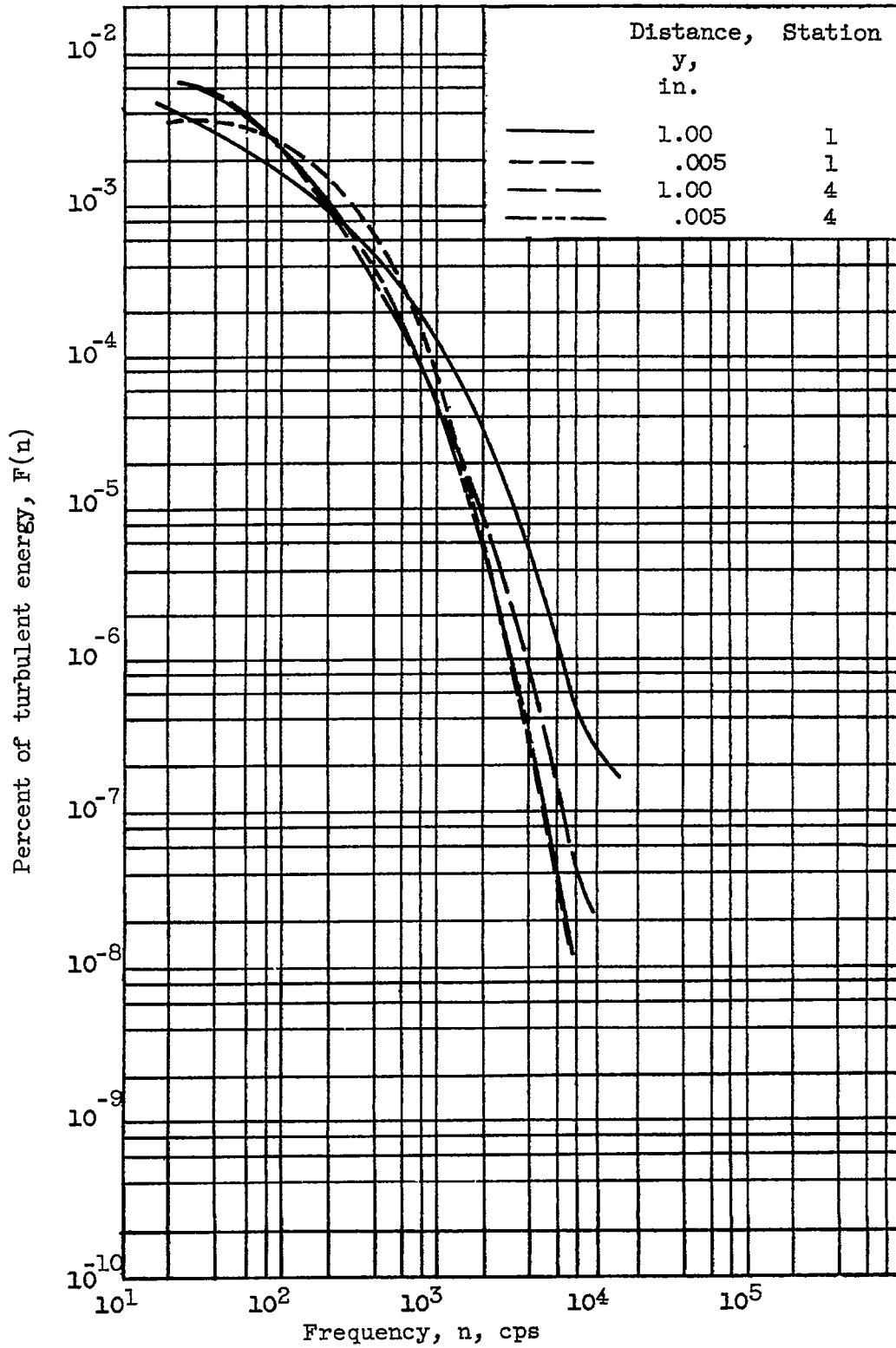
Figure 8. - Comparison between measured spectra at stations
    1 and 4.
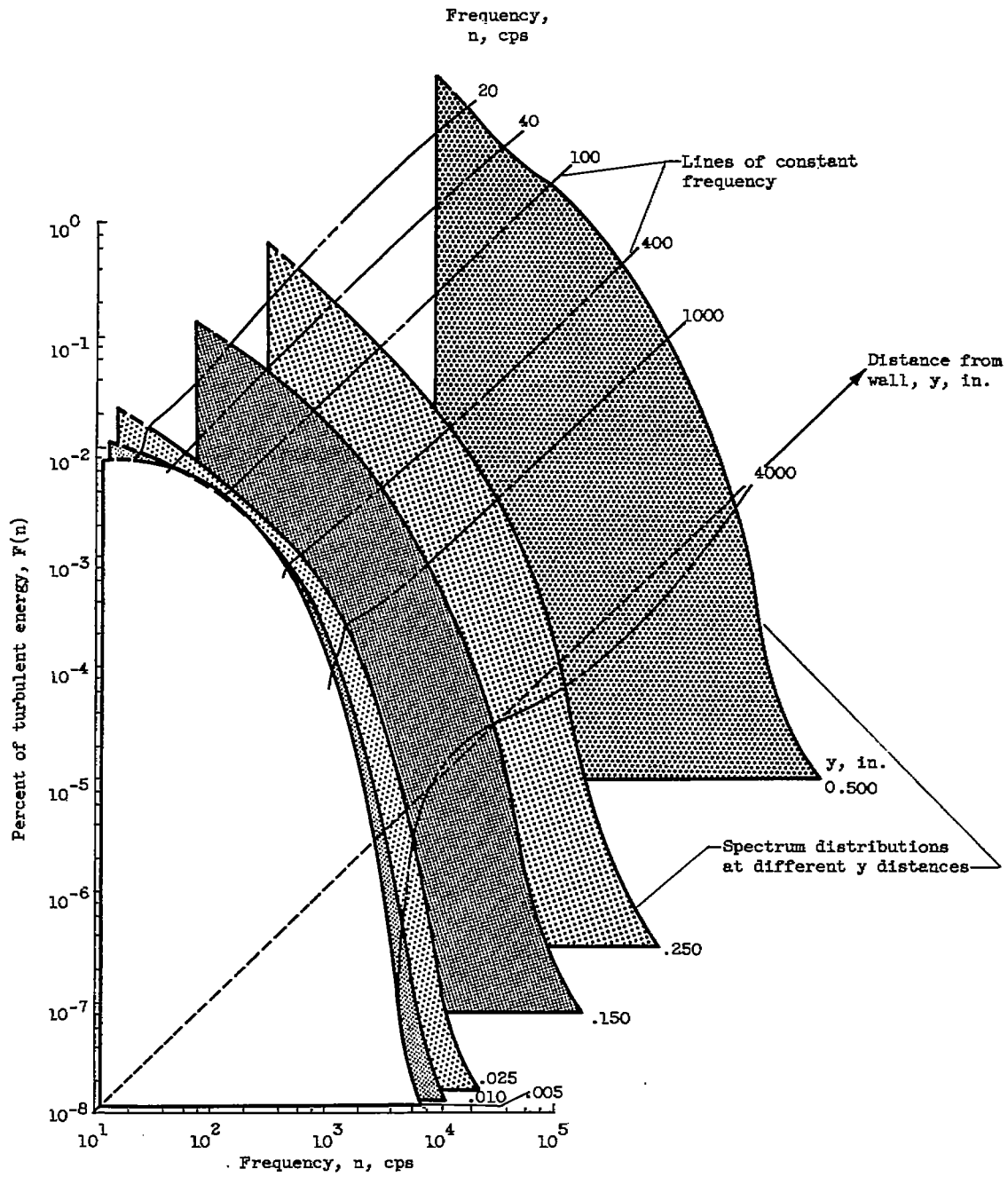
Figure 9. - Three-dimensional plot of longitudinal-turbulent-spectra distribution
near wall, station 2.
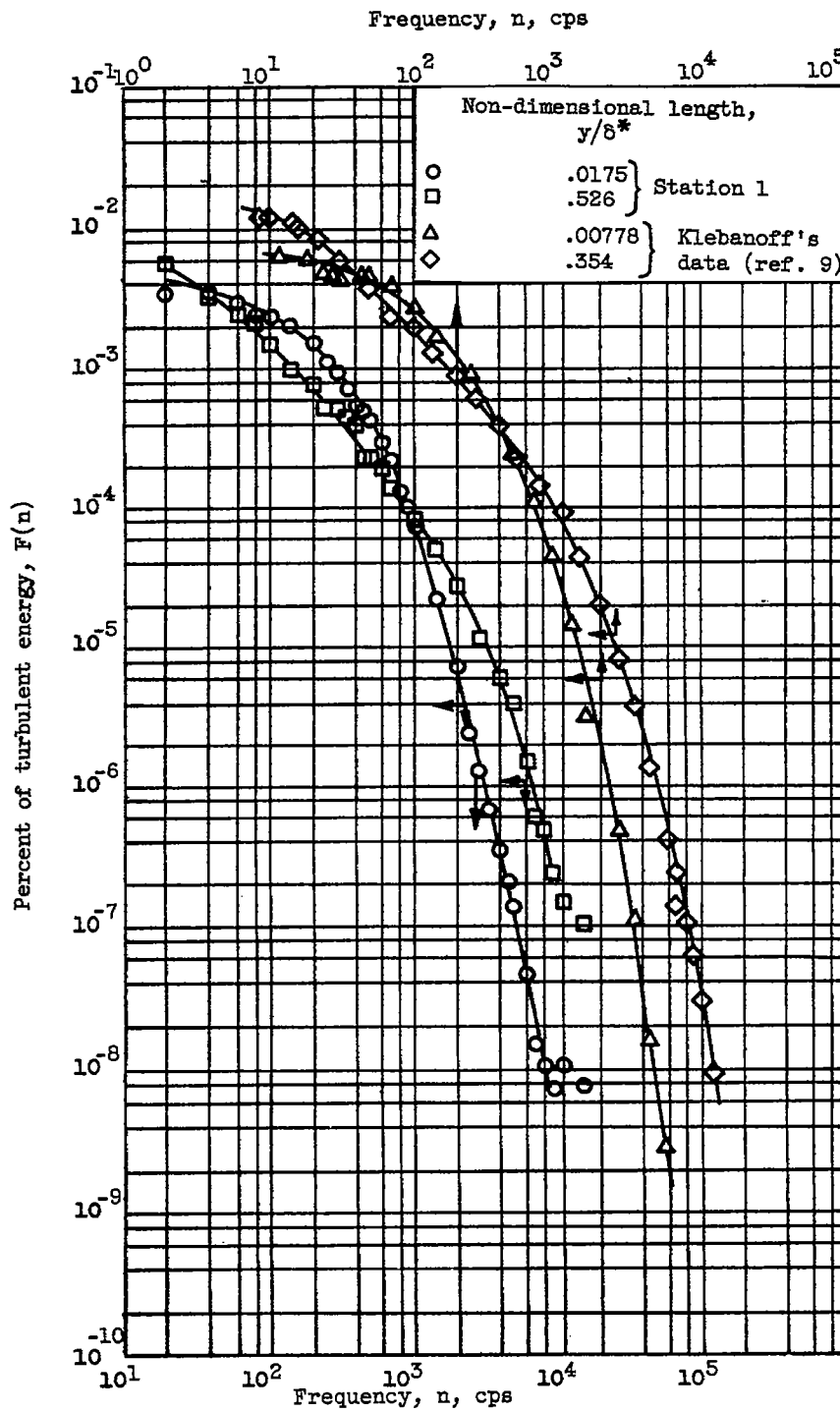
Figure 10. - Comparison of measured longitudinal-turbulent-
spectra distribution with measurements reported by
Klebanoff for a zero-pressure-gradient boundary layer.
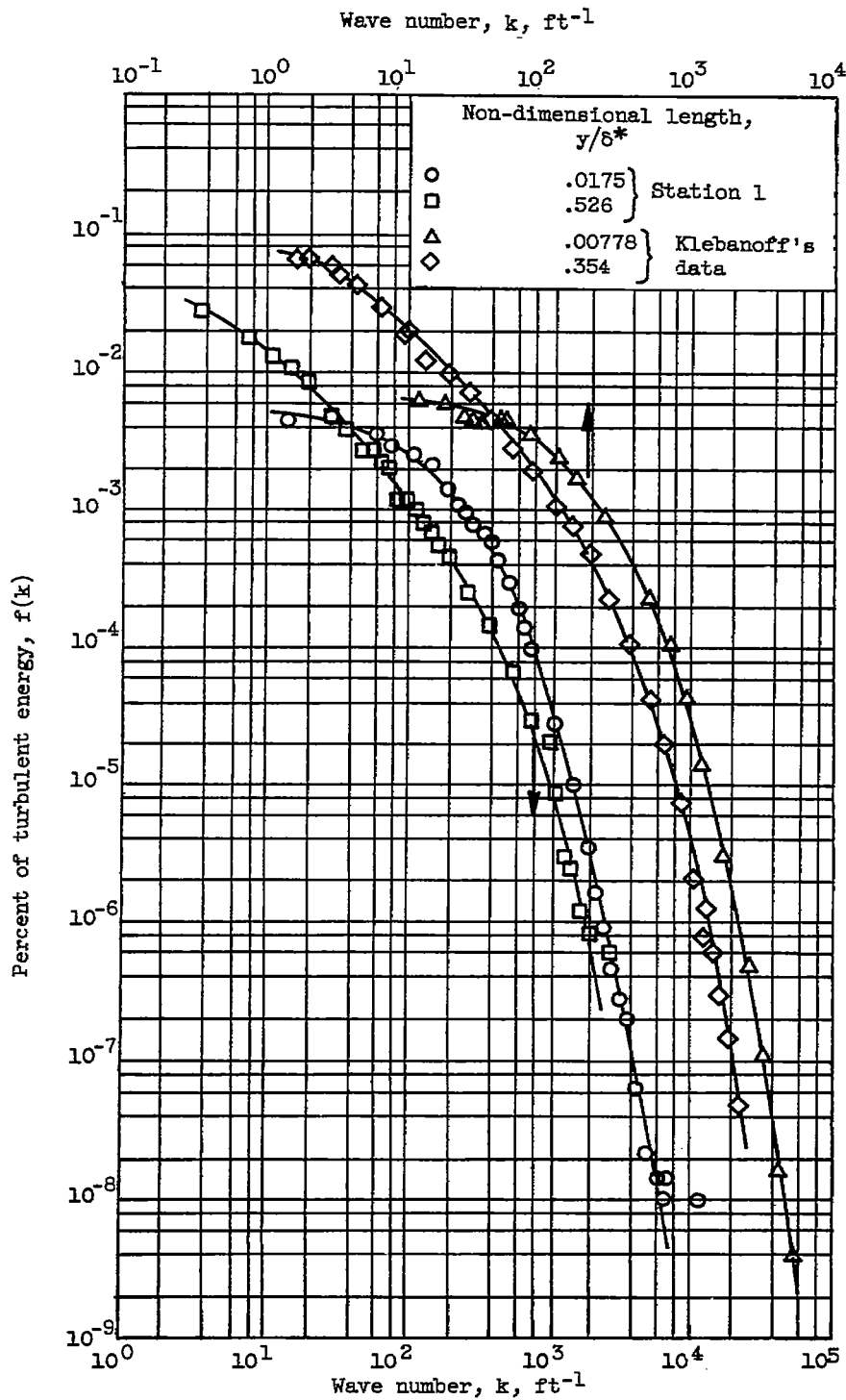
Wave number, k, ft^{-1}

Figure 11. - Comparison of present longitudinal-spectra
measurements in wave number space with those by
Klebanoff (ref. 9).
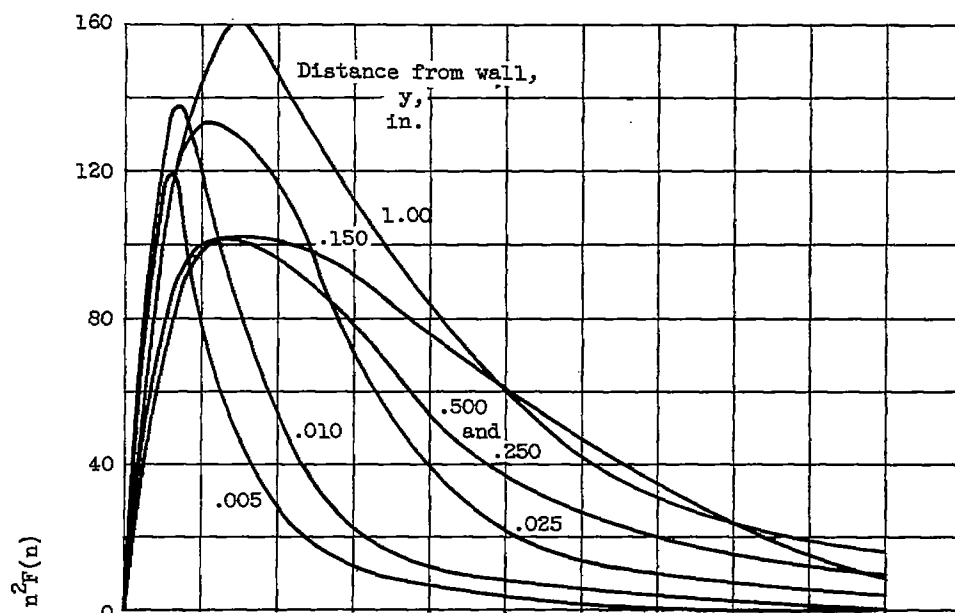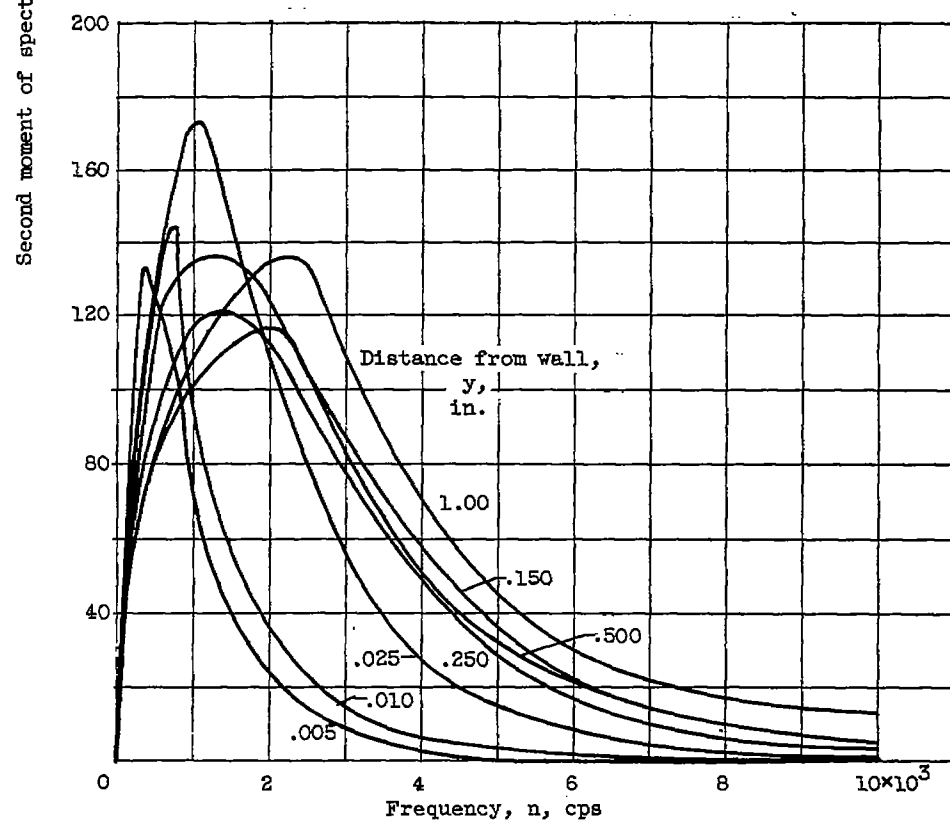
(a) Station 1.

(b) Station 2.

Figure 12. - Variation in boundary layer of second moment of spectra curves.
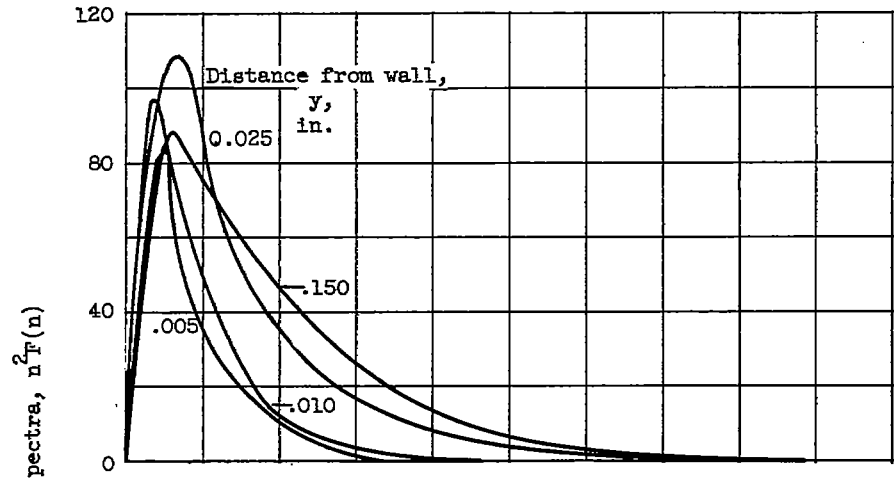
(c) Station 3, region near wall.
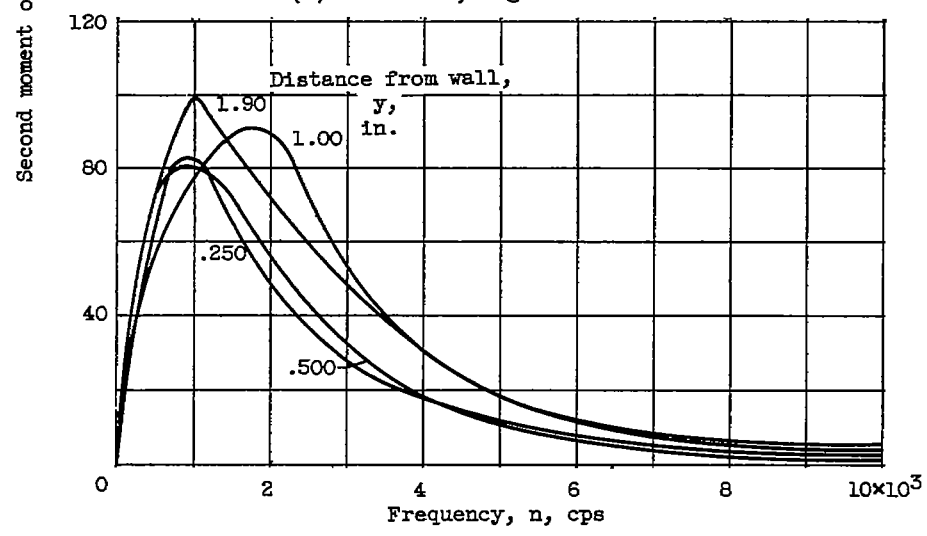
(d) Station 3, outer region.

Figure 12. - Continued. Variation in boundary layer of second
moment of spectra curves.
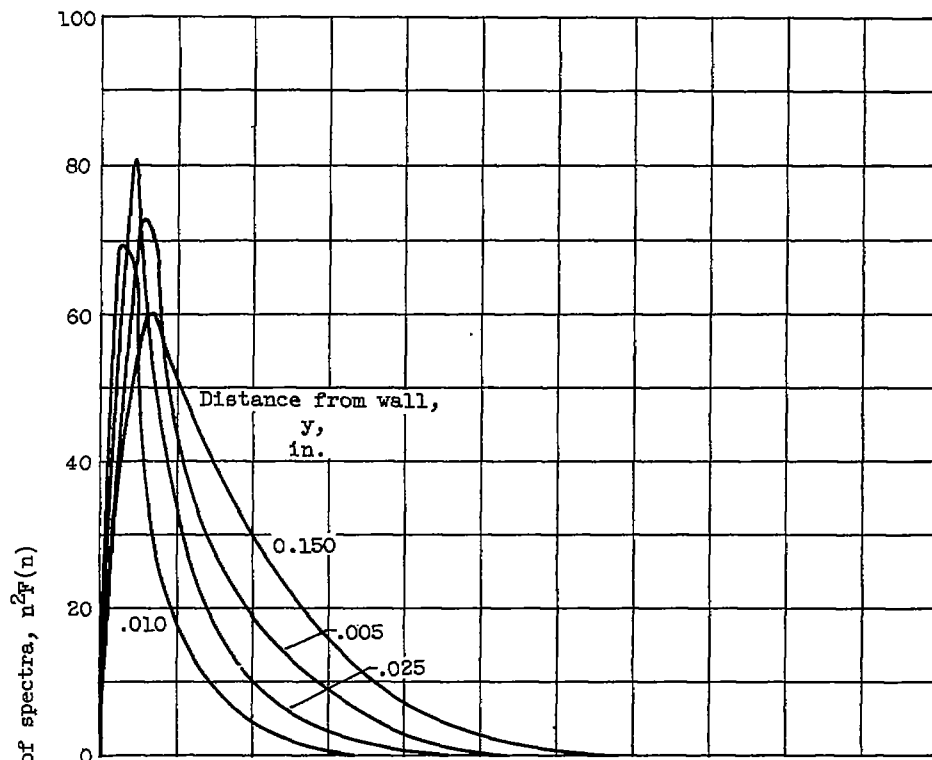
(e) Station 4, region near wall.
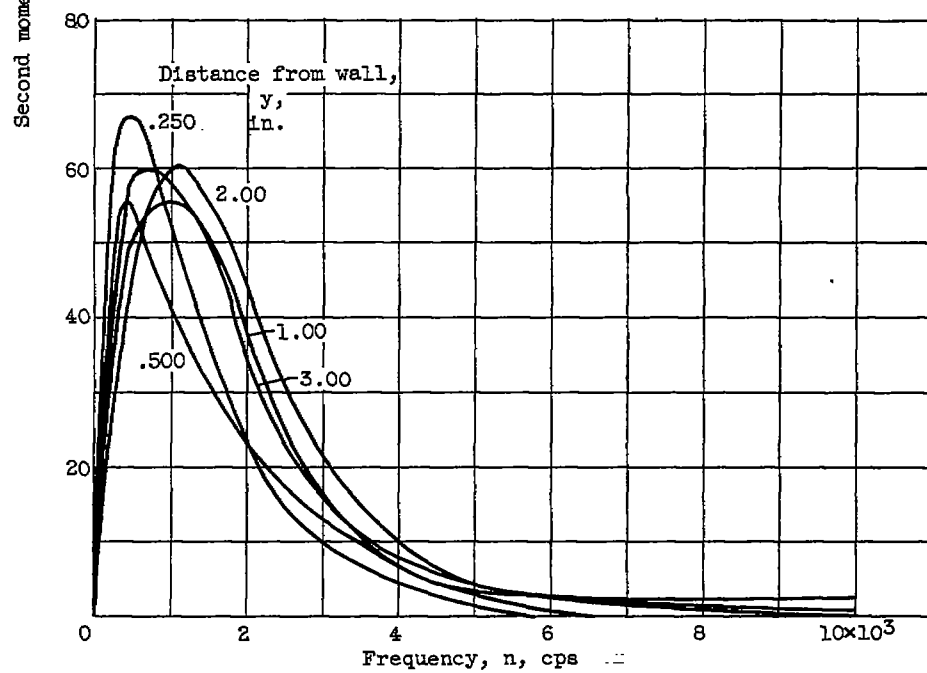
(f) Station 4, outer region.

Figure 12. - Concluded. Variation in boundary layer of second
moment of spectra curves.

(a) Station 1.

(b) Station 2.

(c) Station 3.
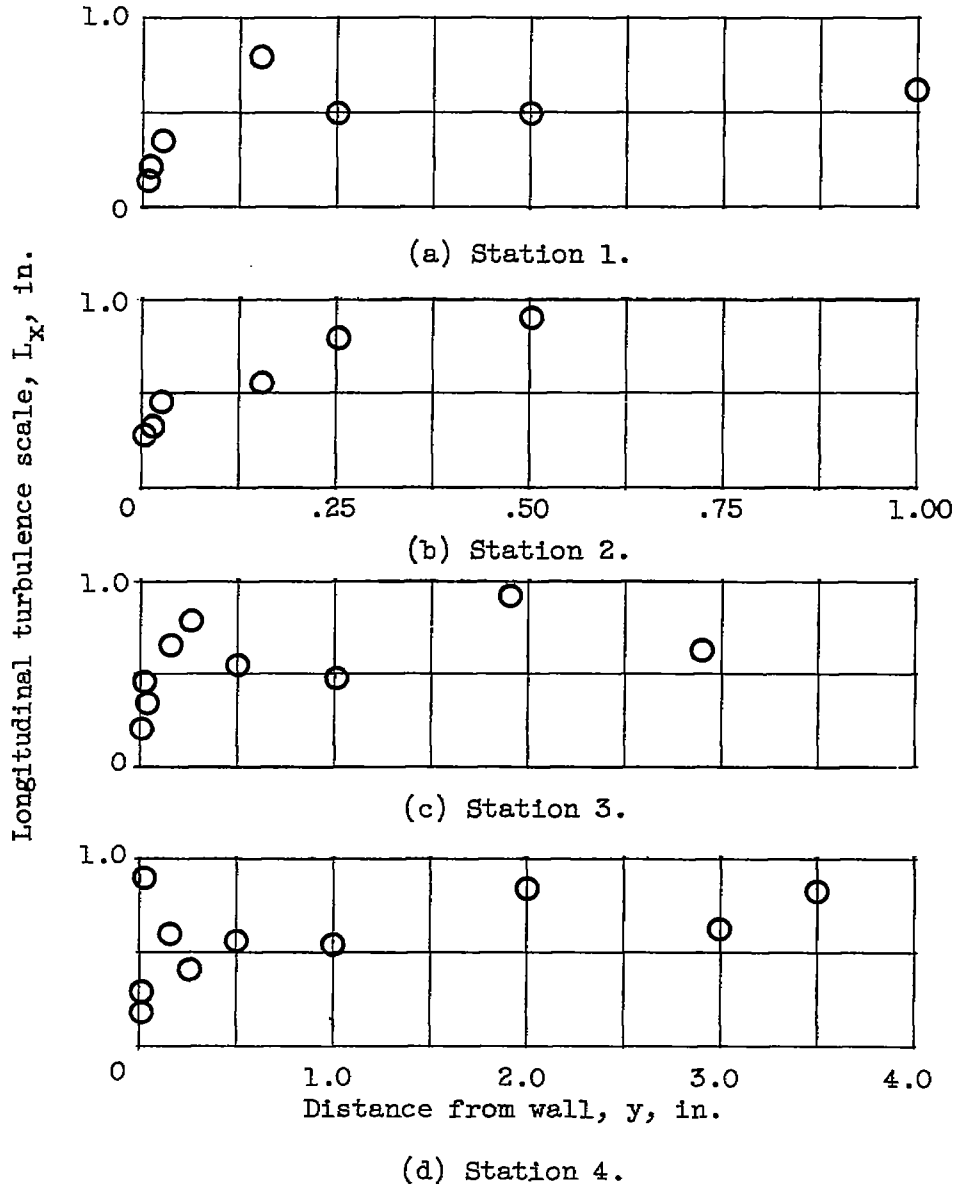
(d) Station 4.

Figure 13. - Variation in boundary layer of longi-
tudinal turbulence scale.
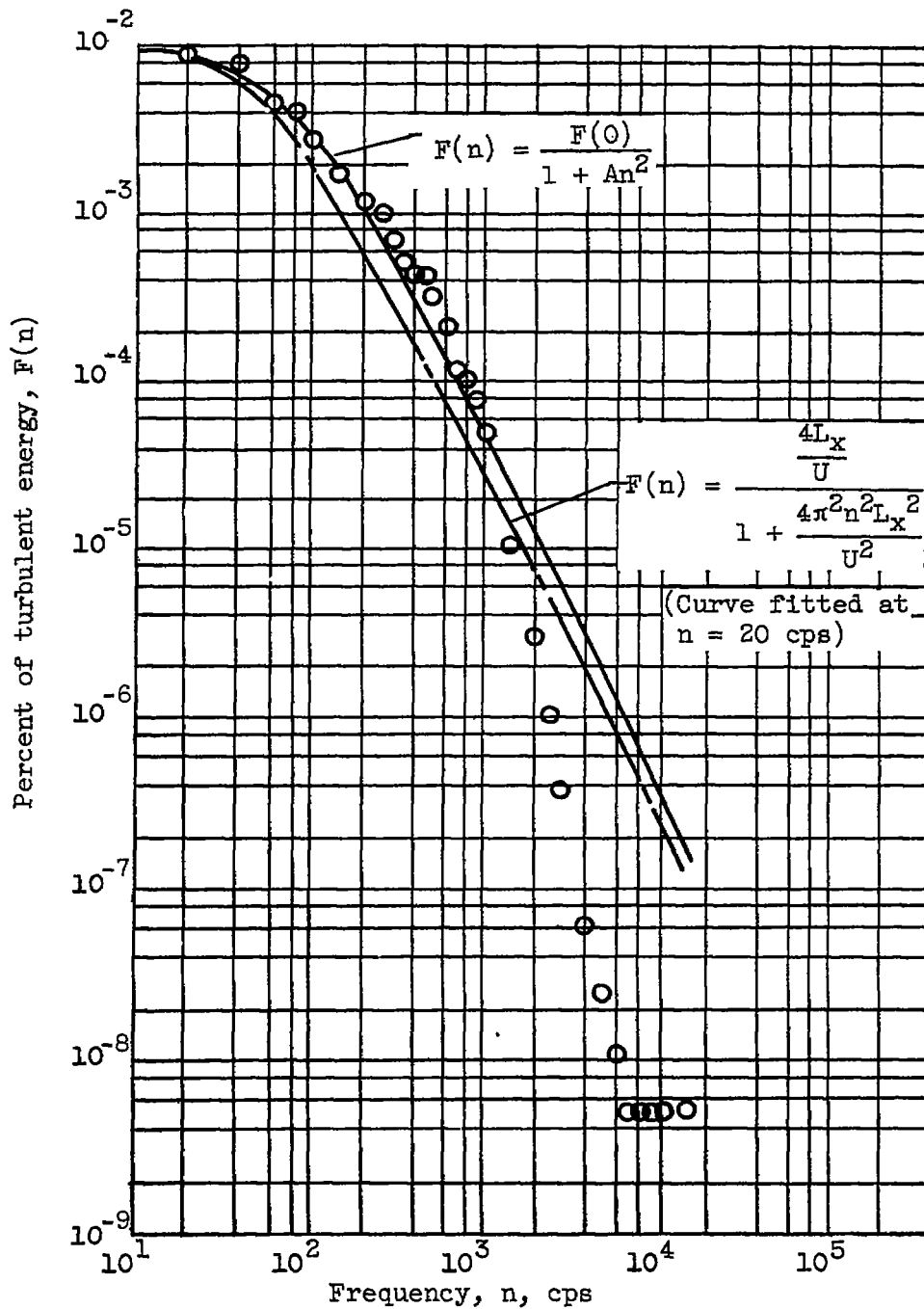
Figure 14. - Comparison of a measured spectrum
curve with curves used to determine longitudinal
turbulence scale. F(0), value of F(n) at n = 0;
distance from tunnel wall at station 3, 0.010 inch.

(a) Station 1.

(b) Station 2.

(c) Station 3.
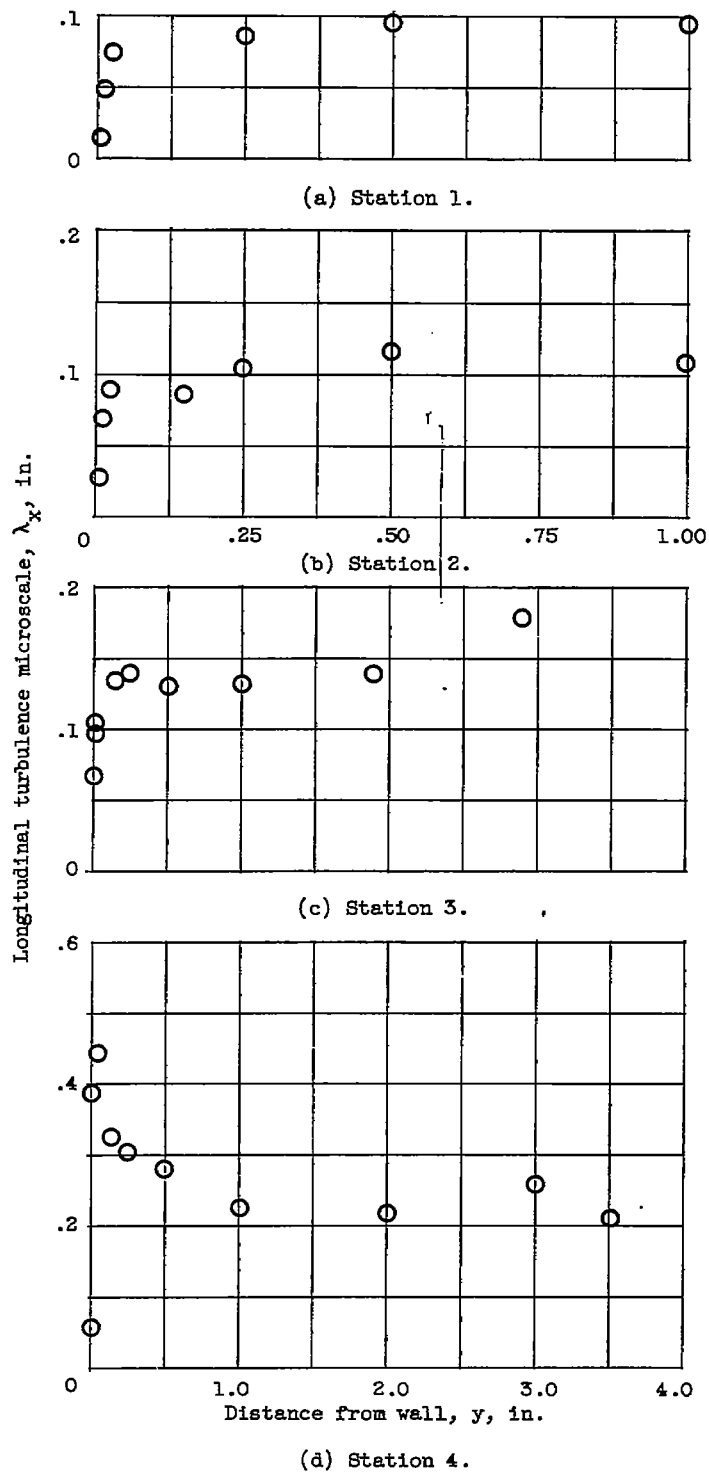
(d) Station 4.

Figure 15. - Variation in boundary layer of longitudinal turbulence microscale.
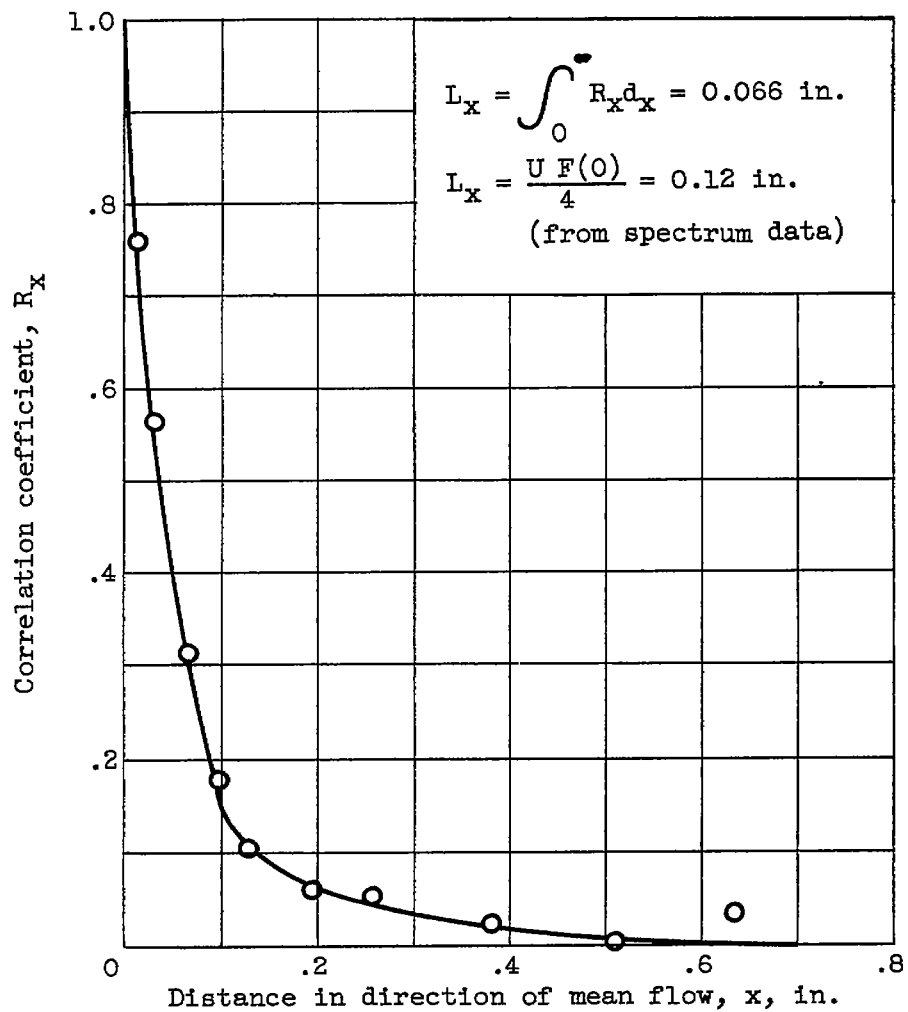
Figure 16. - Evaluation of x-direction correlation
coefficient. Distance from tunnel wall at station
1, 0.005 inch.

3555
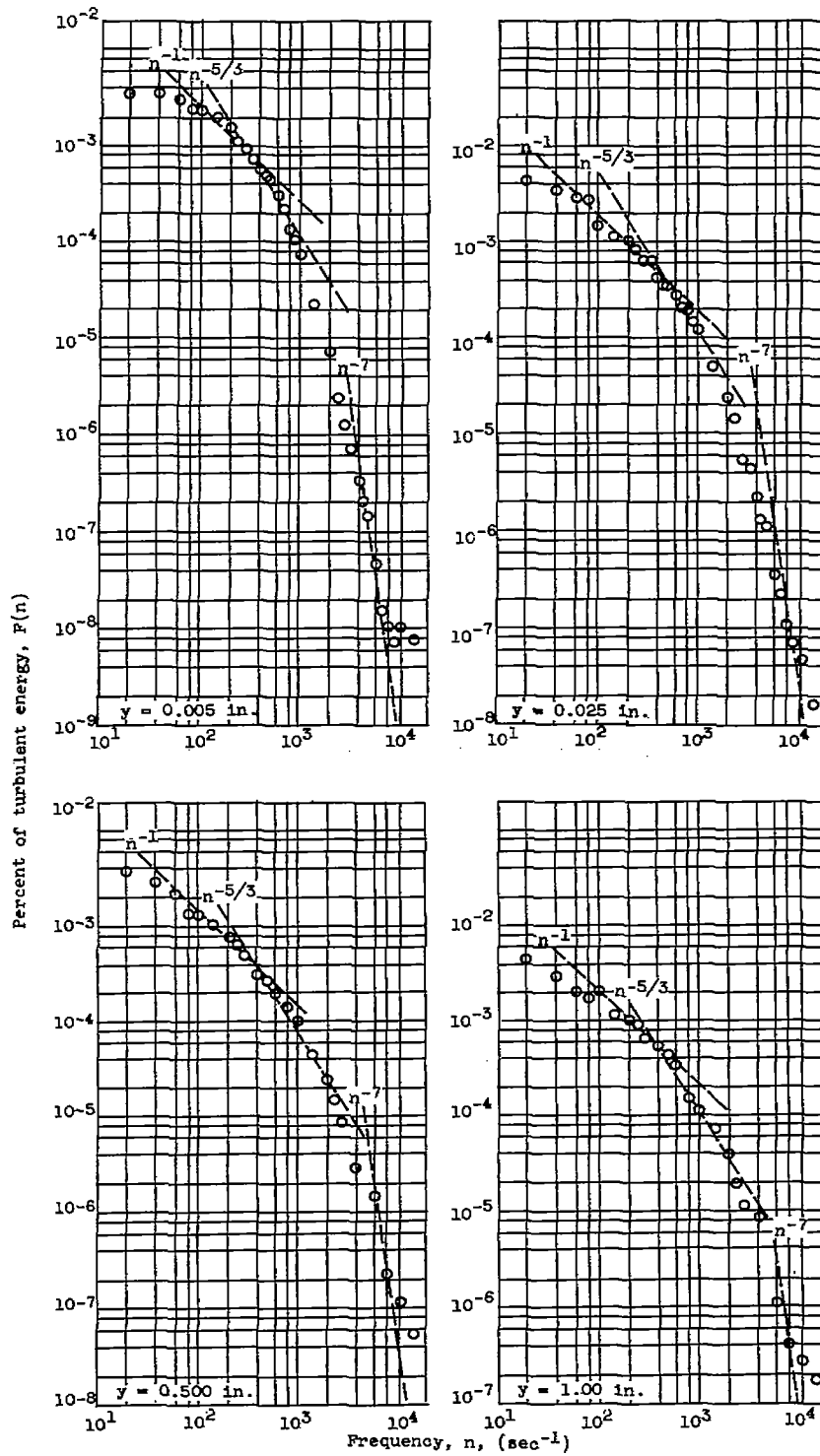
(a) Station 1.

Figure 17 - Spectrum measurements compared with theoretical predictions.

(b) Station 4.
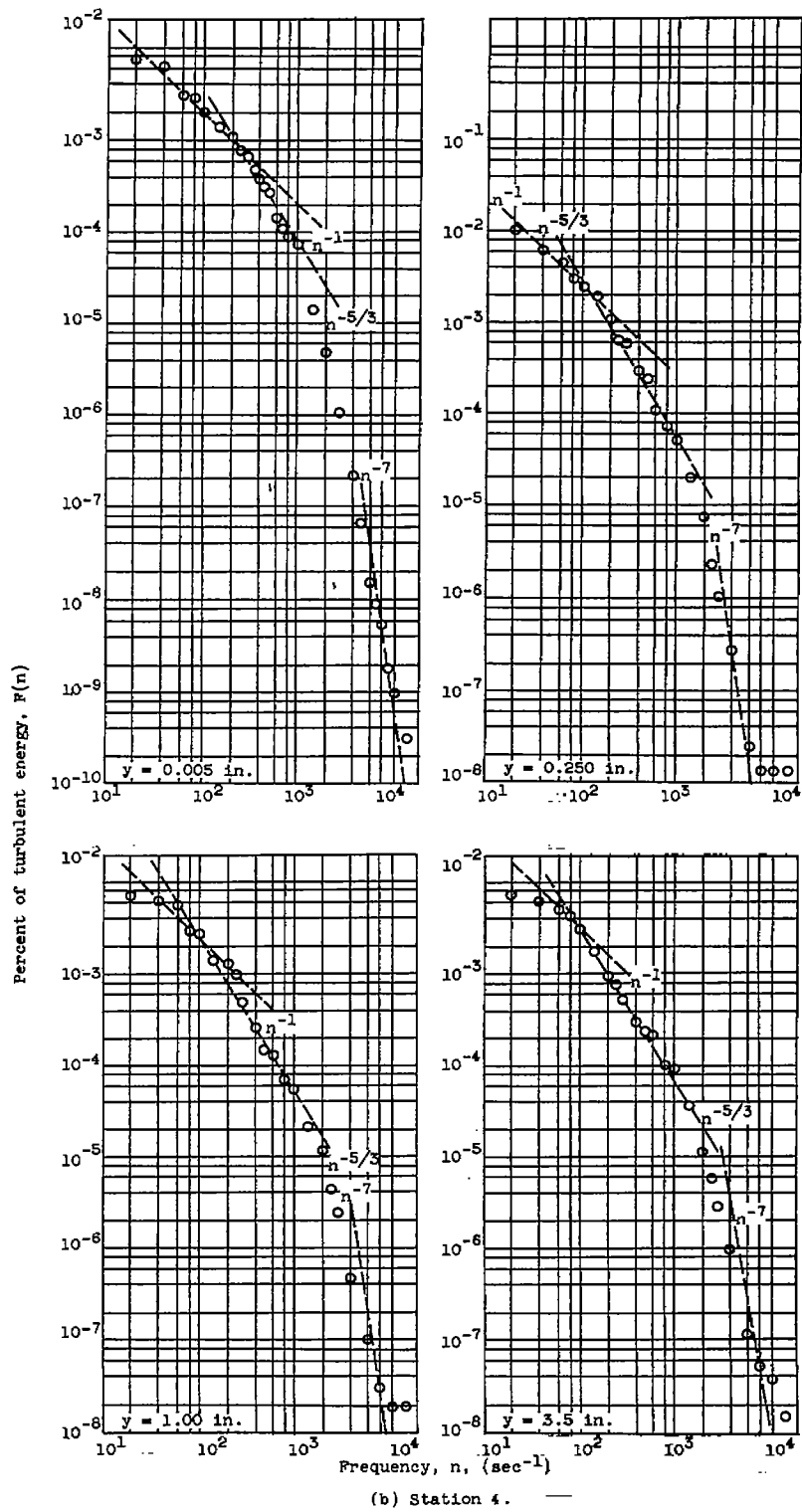
Figure 17. – Concluded. Spectrum measurements compared with theoretical predictions.